NOAA Technical Memorandum NWS WR-199

HEAVY RAINS AND FLOODING IN MONTANA: A CASE FOR SLANTWISE CONVECTION

Glenn R. Lussky

Salt Lake City, Utah
April 1987

U.S. DEPARTMENT OF COMMERCE / National Oceanic and Atmospheric Administration / National Weather Service

NOAA TECHNICAL MEMORANDA
National Weather Service, Western Region Subseries

The National Weather Service (NWS) Western Region (WR) Subseries provides an informal medium for the documentation and quick dissemination of results not appropriate, or not yet ready, for formal publication. The series is used to report on work in progress, to describe technical procedures and practices, or to relate progress to a limited audience. These Technical Memoranda will report on investigations devoted primarily to regional and local problems of interest mainly to personnel, and hence will not be widely distributed.

Papers 1 to 25 are in the former series, ESSA Technical Memoranda, Western Region Technical Memoranda (WRTM); papers 24 to 59 are in the former series, ESSA Technical Memoranda, Weather Bureau Technical Memoranda (WBTM). Beginning with 60, the papers are part of the series, NOAA Technical Memoranda NWS. Out-of-print memoranda are not listed.

Papers 2 to 22, except for 5 (revised edition), are available from the National Weather Service Western Region, Scientific Services Division, P.O. Box 11188, Federal Building, 125 South State Street, Salt Lake City, Utah 84147. Paper 5 (revised edition), and all others beginning with 25 are available from the National Technical Information Service, U.S. Department of Commerce, Sills Building, 5285 Port Royal Road, Springfield, Virginia 22161. Prices vary for all paper copies; $3.50 microfiche. Order by accession number shown in parentheses at end of each entry.

ESSA Technical Memoranda (WRTM)

2 Climatological Precipitation Probabilities. Compiled by Lucianne Miller, December 1965.
3 Western Region Pre- and Post-FP-3 Program, December 1, 1965, to February 20, 1966. Edward D. Diemer, March 1966.
5 Station Descriptions of Local Effects on Synoptic Weather Patterns. Philip Williams, Jr., April 1966 (revised November 1967, October 1969). (PB-17800)
8 Interpreting the RAREP. Herbert P. Benner, May 1966 (revised January 1967).
11 Some Electrical Processes in the Atmosphere. J. Latham, June 1966.
17 A Digitalized Summary of Radar Echoes within 100 Miles of Sacramento, California. J. A. Youngberg and L. B. Overaas, December 1966.
21 An Objective Aid for Forecasting the End of East Winds in the Columbia Gorge, July through October. D. John Coparanis, April 1967.
22 Derivation of Radar Horizons in Mountainous Terrain. Roger G. Pappas, April 1967.

ESSA Technical Memoranda, Weather Bureau Technical Memoranda (WBTM)

25 Verification of Operation Probability of Precipitation Forecasts, April 1966-March 1967. W. W. Dickey, October 1967. (PB-176240)
26 A Study of Winds in the Lake Mead Recreation Area. R. P. Augulis, January 1968. (PB-177830)
28 Weather Extremes. R. J. Schmidli, April 1968 (revised March 1986). (PB86 177672/AS)
29 Small-Scale Analysis and Prediction. Philip Williams, Jr., May 1968. (PB178425)
30 Numerical Weather Prediction and Synoptic Meteorology. CPT Thomas D. Murphy, USAF, May 1968. (AD 673365)
31 Precipitation Detection Probabilities by Salt Lake ARTC Radars. Robert K. Belesky, July 1968. (PB 179084)
32 Probability Forecasting--A Problem Analysis with Reference to the Portland Fire Weather District. Harold S. Ayer, July 1968. (PB 179289)
36 Temperature Trends in Sacramento--Another Heat Island. Anthony D. Lentini, February 1969. (PB 183055)
37 Disposal of Logging Residues Without Damage to Air Quality. Owen P. Cramer, March 1969. (PB 183057)
39 Upper-Air Lows Over Northwestern United States. A.L. Jacobson, April 1969. PB 184296)
40 The Man-Machine Mix in Applied Weather Forecasting in the 1970s. L.W. Snellman, August 1969. (PB 185068)
43 Forecasting Maximum Temperatures at Helena, Montana. David E. Olsen, October 1969. (PB 185762)
44 Estimated Return Periods for Short-Duration Precipitation in Arizona. Paul C. Kangieser, October 1969. (PB 187763)
46 Applications of the Net Radiometer to Short-Range Fog and Stratus Forecasting at Eugene, Oregon. L. Yee and E. Bates, December 1969. (PB 190476)
47 Statistical Analysis as a Flood Routing Tool. Robert J.C. Burnash, December 1969. (PB 188744)
48 Tsunami. Richard P. Augulis, February 1970. (PB 190157)
49 Predicting Precipitation Type. Robert J.C. Burnash and Floyd E. Hug, March 1970. (PB 190962)
50 Statistical Report on Aeroallergens (Pollens and Molds) Fort Huachuca, Arizona, 1969. Wayne S. Johnson, April 1970. (PB 191743)
51 Western Region Sea State and Surf forecaster's Manual. Gordon C. Shields and Gerald B. Burdwell, July 1970. (PB 193102)
52 Sacramento Weather Radar Climatology. R.G. Pappas and C. M. Veliquette, July 1970. (PB 193347)
54 A Refinement of the Vorticity Field to Delineate Areas of Significant Precipitation. Barry B. Aronovitch, August 1970.
55 Application of the SSARR Model to a Basin without Discharge Record. Vail Schermerhorn and Donal W. Kuehl, August 1970. (PB 194394)
56 Areal Coverage of Precipitation in Northwestern Utah. Philip Williams, Jr., and Werner J. Heck, September 1970. (PB 194389)
57 Preliminary Report on Agricultural Field Burning vs. Atmospheric Visibility in the Willamette Valley of Oregon. Earl M. Bates and David O. Chilcote, September 1970. (PB 194710)
58 Air Pollution by Jet Aircraft at Seattle-Tacoma Airport. Wallace R. Donaldson, October 1970. (COM 71 00017)
59 Application of PE Model Forecast Parameters to Local-Area Forecasting. Leonard W. Snellman, October 1970. (COM 71 00016)

NOAA Technical Memoranda (NWS WR)

60 An Aid for Forecasting the Minimum Temperature at Medford, Oregon, Arthur W. Fritz, October 1970. (COM 71 00120)
63 700-mb Warm Air Advection as a Forecasting Tool for Montana and Northern Idaho. Norris E. Woerner, February 1971. (COM 71 00349)
64 Wind and Weather Regimes at Great Falls, Montana. Warren B. Price, March 1971.
66 A Preliminary Report on Correlation of ARTCC Radar Echoes and Precipitation. Wilbur K. Hall, June 1971. (COM 71 00829)
69 National Weather Service Support to Soaring Activities. Ellis Burton, August 1971. (COM 71 00956)
71 Western Region Synoptic Analysis-Problems and Methods. Philip Williams, Jr., February 1972. (COM 72 10433)
74 Thunderstorms and Hail Days Probabilities in Nevada. Clarence M. Sakamoto, April 1972. (COM 72 10554)
75 A Study of the Low Level Jet Stream of the San Joaquin Valley. Ronald A. Willis and Philip Williams, Jr., May 1972. (COM 72 10707)
76 Monthly Climatological charts of the Behavior of Fog and Low Stratus at Los Angeles International Airport. Donald M. Gales, July 1972. (COM 72 11140)
77 A Study of Radar Echo Distribution in Arizona During July and August. John E. Hales, Jr., July 1972. (COM 72 11136)
78 Forecasting Precipitation at Bakersfield, California, Using Pressure Gradient Vectors. Earl T. Riddiough, July 1972. (COM 72 11146)
79 Climate of Stockton, California. Robert C. Nelson, July 1972. (COM 72 10920)
80 Estimation of Number of Days Above or Below Selected Temperatures. Clarence M. Sakamoto, October 1972. (COM 72 10021)
81 An Aid for Forecasting Summer Maximum Temperatures at Seattle, Washington. Edgar G. Johnson, November 1972. (COM 73 10150)
82 Flash Flood Forecasting and Warning Program in the Western Region. Philip Williams, Jr., Chester L. Glenn, and Roland L. Raetz, December 1972, (revised March 1978). (COM 73 10251)
83 A comparison of Manual and Semiautomatic Methods of Digitizing Analog Wind Records. Glenn E. Rasch, March 1973. (COM 73 10669)
86 Conditional Probabilities for Sequences of Wet Days at Phoenix, Arizona. Paul C. Kangieser, June 1973. (COM 73 11264)
87 A Refinement of the Use of K-Values in Forecasting Thunderstorms in Washington and Oregon. Robert Y.G. Lee, June 1973. (COM 73 11276)
89 Objective Forecast Precipitation Over the Western Region of the United States. Julia N. Paegle and Larry P. Kierulff, September 1973. (COM 73 11946/3AS)
91 Arizona "Eddy" Tornadoes. Robert S. Ingram, October 1973. (COM 73 10465)
92 Smoke Management in the Willamette Valley. EArl M. Bates, May 1974. (COM 74 11277/AS)
93 An Operational Evaluation of 500-mb Type Regression Equations. Alexander E. MacDonald, June 1974. (COM 74 11407/AS)
94 Conditional Probability of Visibility Less than One-Half Mile in Radiation Fog at Fresno, California. John D. Thomas, August 1974. (COM 74 11555/AS)
95 Climate of Flagstaff, Arizona. Paul W. Sorenson, and updated by Reginald W. Preston, January 1987. (PB87 143160/AS)
96 Map type Precipitation Probabilities for the Western Region. Glenn E. Rasch and Alexander E. MacDonald, February 1975. (COM 75 10428/AS)
97 Eastern Pacific Cut-Off Low of April 24-28, 1974. William J. Alder and George R. Miller, January 1976. (PB 250 711/AS)
98 Study on a Significant Precipitation Episode in Western United States. Ira S. Brenner, April 1976. (COM 75 10719/AS)
99 A Study of Flash Flood Susceptibility-A Basin in Southern Arizona. Gerald Williams, August 1975. (COM 75 11360/AS)
102 A Set of Rules for Forecasting Temperatures in Napa and Sonoma Counties. Wesley L. Tuft, October 1975. (PB 246 902/AS)
103 Application of the National Weather Service Flash-Flood Program in the Western Region. Gerald Williams, January 1976. (PB 253 053/AS)
104 Objective Aids for Forecasting Minimum Temperatures at Reno, Nevada, During the Summer Months. Christopher D. Hill, January 1976. (PB 252 866/AS)
105 Forecasting the Mono Wind. Charles P. Ruscha, Jr., February 1976. (PB 254 650)
106 Use of MOS Forecast Parameters in Temperature Forecasting. John C. Plankinton, Jr., March 1976. (PB 254 649)
107 Map Types as Aids in Using MOS PoPs in Western United States. Ira S. Brenner, August 1976. (PB 259 594)
108 Other Kinds of Wind Shear. Christopher D. Hill, August 1976. (PB 260 437/AS)
109 Forecasting North Winds in the Upper Sacramento Valley and Adjoining Forests. Christopher E. Fontana, September 1976. (PB 273 677/AS)
110 Cool Inflow as a Weakening Influence on Eastern Pacific Tropical Cyclones. William J. Denney, November 1976. (PB 264 655/AS)
112 The MAN/MOS Program. Alexander E. MacDonald, February 1977. (PB 265 941/AS)
113 Winter Season Minimum Temperature Formula for Bakersfield, California, Using Multiple Regression. Michael J. Oard, February 1977. (PB 273 694/AS)
114 Tropical Cyclone Kathleen. James R. Fors, February 1977. (PB 273 675/AS)
116 A Study of Wind Gusts on Lake Mead. Bradley Colman, April 1977. (PB 268 847)
117 The Relative Frequency of Cumulonimbus Clouds at the Nevada Test Site as a Function of K-Value. R.F. Quiring, April 1977. (PB 272 831)
118 Moisture Distribution Modification by Upward Vertical Motion. Ira S. Brenner, April 1977. (PB 268 740)
119 Relative Frequency of Occurrence of Warm Season Echo Activity as a Function of Stability Indices Computed from the Yucca Flat, Nevada, Rawinsonde. Darryl Randerson, June 1977. (PB 271 290/AS)
121 Climatological Prediction of Cumulonimbus Clouds in the Vicinity of the Yucca Flat Weather Station. R.F. Quiring, June 1977. (PB 271 704/AS)
122 A Method for Transforming Temperature Distribution to Normality. Morris S. Webb, Jr., June 1977. (PB 271 742/AS)
124 Statistical Guidance for Prediction of Eastern North Pacific Tropical Cyclone Motion - Part I. Charles J. Neumann and Preston W. Leftwich, August 1977. (PB 272 661)
125 Statistical Guidance on the Prediction of Eastern North Pacific Tropical Cyclone Motion - Part II. Preston W. Leftwich and Charles J. Neumann, August 1977. (PB 273 155/AS)
127 Development of a Probability Equation for Winter-Type Precipitation Patterns in Great FAlls, Montana. Kenneth B. Mielke, February 1978. (PB 281 387/AS)
128 Hand Calculator Program to Compute Parcel Thermal Dynamics. Dan Gudgel, April 1978. (PB 283 080/AS)
129 Fire whirls. David W. Goens, May 1978. (PB 283 866/AS)
130 Flash-Flood Procedure. Ralph C. Hatch and Gerald Williams, May 1978. (PB 286 014/AS)
131 Automated Fire-Weather Forecasts. Mark A. Mollner and David E. Olsen, September 1978. (PB 289 916/AS)
132 Estimates of the Effects of Terrain Blocking on the Los Angeles WSR-74C Weather Radar. R.G. Pappas, R.Y. Lee, B.W. Finke, October 1978. (PB 289767/AS)
133 Spectral Techniques in Ocean Wave Forecasting. John A. Jannuzzi, October 1978. (PB291317/AS)
134 Solar Radiation. John A. Jannuzzi, November 1978. (PB291195/AS)
135 Application of a Spectrum Analyzer in Forecasting Ocean Swell in Southern California Coastal Waters. Lawrence P. Kierulff, January 1979. (PB292716/AS)
136 Basic Hydrologic Principles. Thomas L. Dietrich, January 1979. (PB292247/AS)
137 LFM 24-Hour Prediction of Eastern Pacific Cyclones Refined by Satellite Images. John R. Zimmerman and Charles P. Ruscha, Jr., January 1979. (PB294324/AS)
138 A Simple Analysis/Diagnosis System for Real Time Evaluation of Vertical Motion. Scott Heflick and James R. Fors, February 1979. (PB294216/AS)

NOAA Technical Memorandum NWS WR-199

HEAVY RAINS AND FLOODING IN MONTANA: A CASE FOR SLANTWISE CONVECTION

Glenn R. Lussky

National Weather Service Western Region Headquarters
Scientific Services Division
Salt Lake City, Utah
April 1987

UNITED STATES
DEPARTMENT OF COMMERCE
Malcolm Baldrige, Secretary

National Oceanic and
Atmospheric Administration
John V. Byrne, Administrator

National Weather
Service
Richard E. Hallgren, Director

This publication has been reviewed
and is approved for publication by
Scientific Services Division,
Western Region.

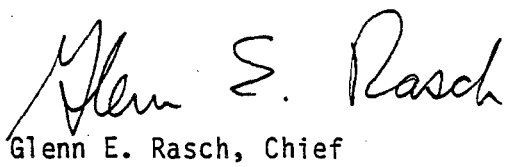

Glenn E. Rasch, Chief
Scientific Services Division
Western Region Headquarters
Salt Lake City, Utah

TABLE OF CONTENTS

LIST OF TABLES

LIST OF FIGURES

HEAVY RAINS AND FLOODING IN MONTANA: A CASE FOR SLANTWISE CONVECTION

ABSTRACT

A strongly developing cyclone east of the Rockies moved northward along the Montana/North Dakota border and deposited an inch or more of precipitation throughout eastern Montana. Embedded in this precipitation area was a heavy band, with rainfall amounts exceeding 7 inches over a 24 to 36 hour period. Kinematic vertical velocity profiles are examined. The possible roles played by frontogenesis and symmetric instability are investigated. The potential operational use of symmetric instability concepts, for both diagnostics and prediction, are discussed with respect to today's operational environment and that of the future.

HEAVY RAINS AND FLOODING IN MONTANA: A CASE FOR SLANTWISE CONVECTION

I. INTRODUCTION

During the week of September 22, 1986, an unseasonably strong upper level trough developed over western North America. As this pattern evolved, the remains of Hurricane Newton moved across central Texas into the midwest and moisture from tropical storm Madeline became entrained into the western states. The result was copious rainfall for much of the region and several severe weather events such as tornadoes in northern California and high winds in Utah and Montana.

The most devastating aspect of this storm, however, was probably the flooding event that occurred in Montana. There, moisture from both of the tropical storms was combined to produce rainfall amounts between 5 and 8 inches over an approximately 4800 mi^2 (12,442 km^2) area between Havre and Glasgow in north-central Montana. The heaviest rains fell between 11:00 p.m. MDT September 24 and 8:00 a.m. MDT (0500 to 1400 UTC) September 25. This heavy rain event caused several rivers and streams to overflow their banks with record to near-record flooding that lasted for several days.

This paper has four main sections. First, it will review the synoptic development and observations associated with this storm. Secondly, it examines the performance of the short-term numerical models, with emphasis mainly on the model development of the surface system (due to its implications on low-level convergence) and the model precipitation forecasts. Third, it discusses some of the physical processes that may have been involved in producing this heavy rain event. Finally, a summary of the main points are presented.

II. OBSERVATIONS

A. Large Scale

Early in the week prior to this heavy rain event, the large scale was characterized by a split in the eastern Pacific with a closed low forming along the California coast in the southern branch of the flow (Figure 1). The Medium Range Forecast (MRF) model predicted that the low would move southeastward and then open up and move eastward in response to the development of a full latitude trough along or just off the west coast (Figure 2). The Western Region prognostic map discussion (PMD) from the 22nd stated:

> "...MRF forecasts the split to change into a full latitude trough ... around 125 to 130W. Have no quarrel with this solution."

Fig. 1. 500 mb hemispheric initial height analysis 0000 UTC September 22.

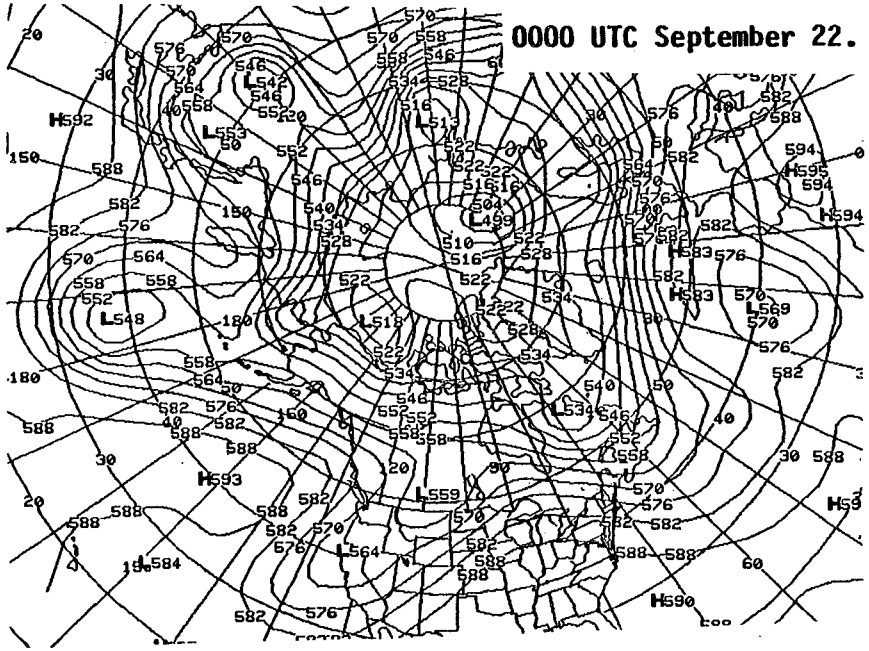

Fig. 2. MRF 96-hour forecast of 500 mb heights valid 0000 UTC September 26.

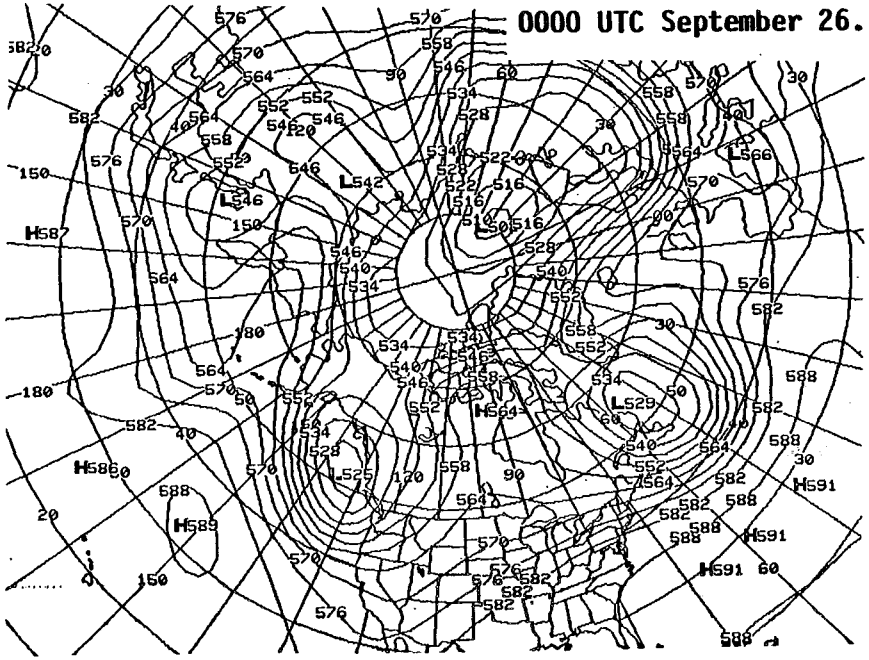

Fig. 3. 500 mb hemispheric initial height analysis 0000 UTC September 26.

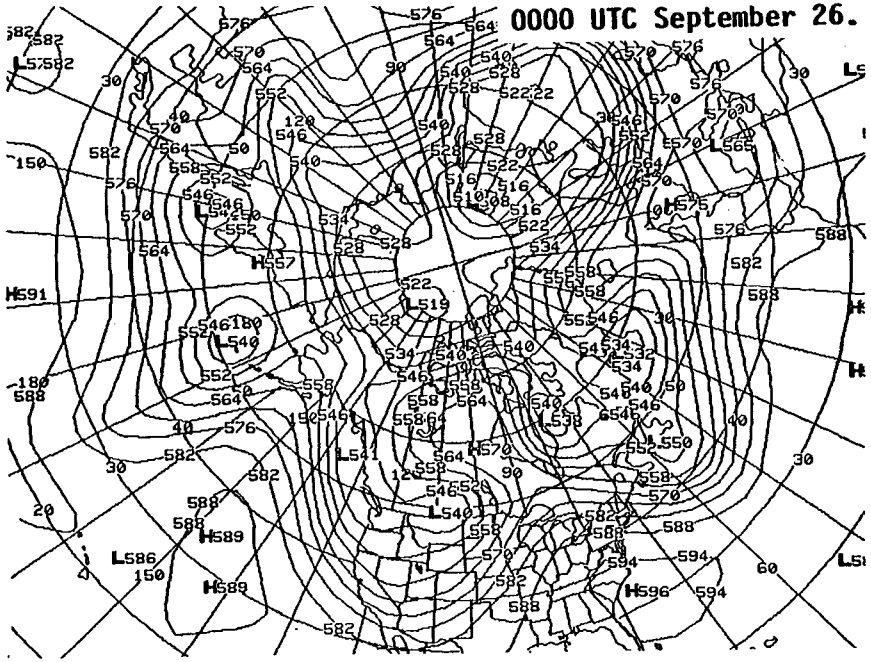

It seemed a reasonable solution in light of the apparent retrogression of the upstream trough in the western Pacific. The MRF, however, had been having a difficult time handling some of the changes across the Pacific. Verification showed that the original trough near the dateline continued as a persistent feature throughout the week. As a result, the full latitude trough that developed later in the week was centered over western North America - farther east than the MRF had predicted (Figure 3). Apparently, the key to the model error was the poor handle it had on the upstream flow pattern. Otherwise, the model correctly predicted the development of a full latitude trough near the west coast over several runs, including the one as shown in figure 2.

B. Synoptic Scale

A series of 2-mile infrared satellite pictures (Figure 4) and corresponding 500 mb (Figure 5) and sea level pressure analyses (Figure 6) are shown for the 36-hour period leading up to 1200 UTC September 25.

By 0000 UTC September 24, moisture from the remains of tropical storm Madeline was entrained into the southwest, primarily into Arizona and Utah. The moist band can be seen in the IR satellite image (Figure 4a) extending from about 20N/130W northeastward into Utah. Also evident from Texas to Nebraska is convection which resulted from the northeasterly movement of moisture from hurricane Newton. The low that earlier formed along the northern California coast had moved into the Los Angeles basin. During the next 12 hours, it accelerated eastward into western Arizona in response to the digging short-wave trough along the Pacific northwest coast (Figure 5b). By 0000 UTC September 25, the open trough remains of the original closed low were approaching southeastern Wyoming (Figure 5c). By 1200 UTC September 25, the associated vorticity center had moved northward along the eastern Montana border and intensified (Figure 5d).

At the surface, a closed 986 mb low formed by 0000 UTC September 25 east of the Rockies in eastern Wyoming and eastern Montana (Figure 6c). This low moved straight northward and intensified dramatically to a 974 mb central pressure during the next 12 hours (Figure 6d). It was during the last 12-hour period that heavy rains began in eastern and north-central Montana. An inverted trough extended to the northwest from the surface low center, parallel to and along the heavy rain axis. It is hypothesized that this trough played an important role in the location and intensity of the observed heavy rainfall.

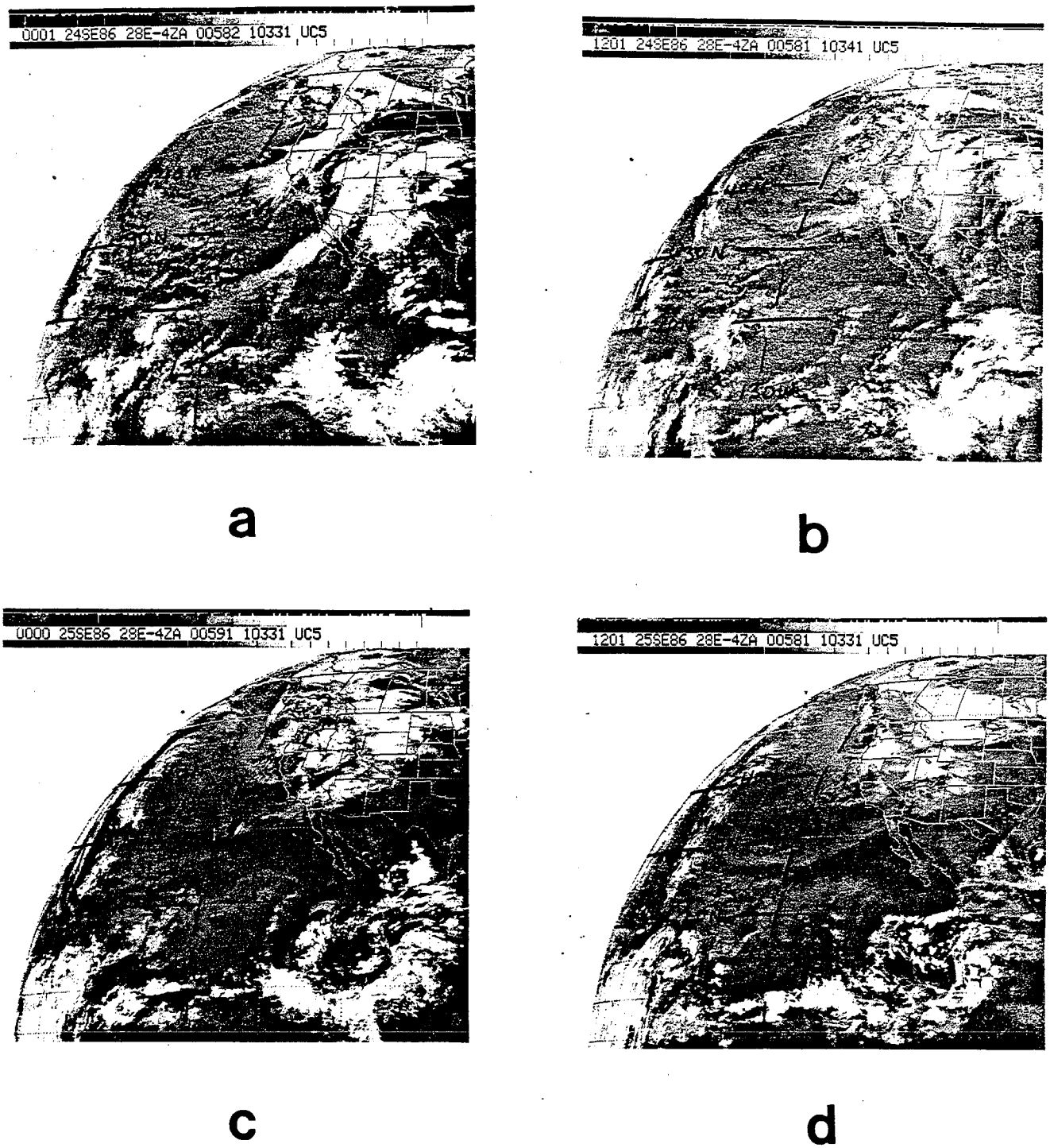

Fig. 4. 2-mile IR satellite sequence for a) 0000 UTC September 24, b) 1200 September 24, c) 0000 UTC September 25 and d) 1200 UTC September 25.

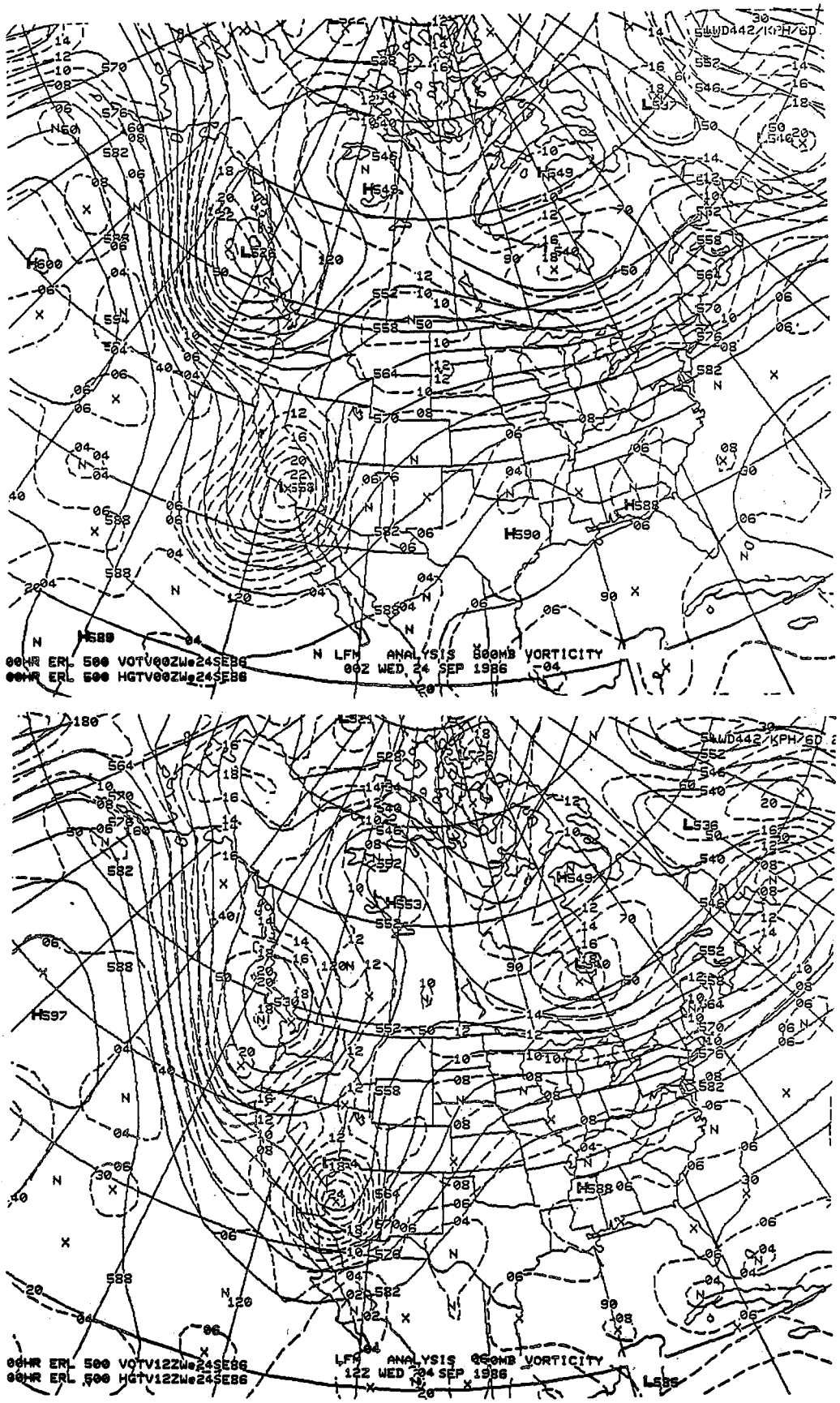

Fig. 5. LFM 500 mb height and vorticity initial analyses for a) 0000 UTC September 24, b) 1200 UTC September 24, c) 0000 UTC September 25 and d) 1200 UTC September 25.

c

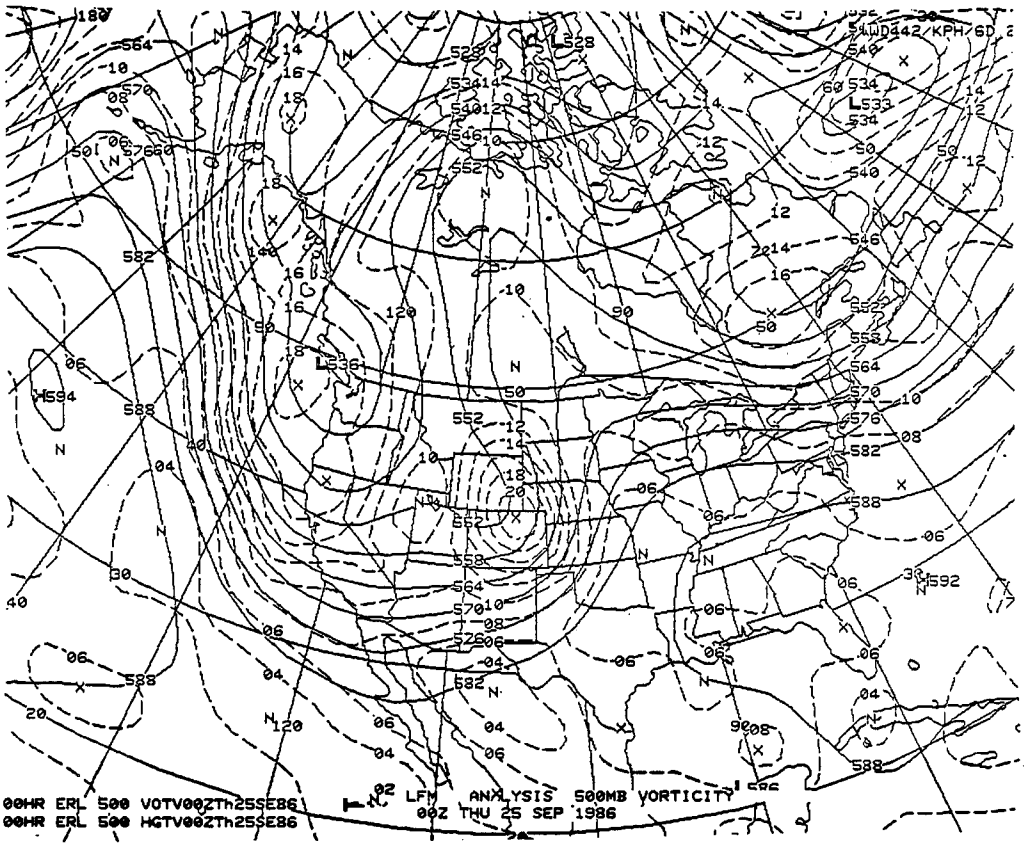
00HR ERL 500 VOTV00ZTh25SE86
00HR ERL 500 HGTV00ZTh25SE86
LFM ANALYSIS 500MB VORTICITY
00Z THU 25 SEP 1986

d

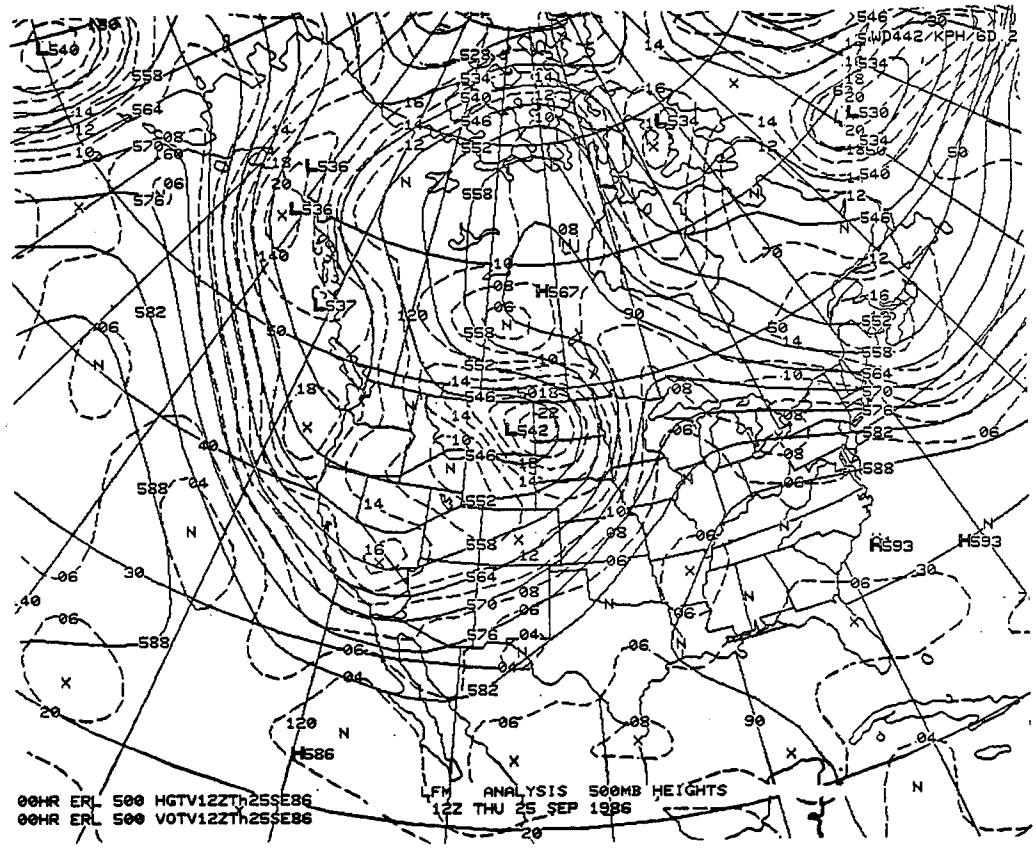
00HR ERL 500 HGTV12ZTh25SE86
00HR ERL 500 VOTV12ZTh25SE86
LFM ANALYSIS 500MB HEIGHTS
12Z THU 25 SEP 1986

Fig. 5 (cont.)

a

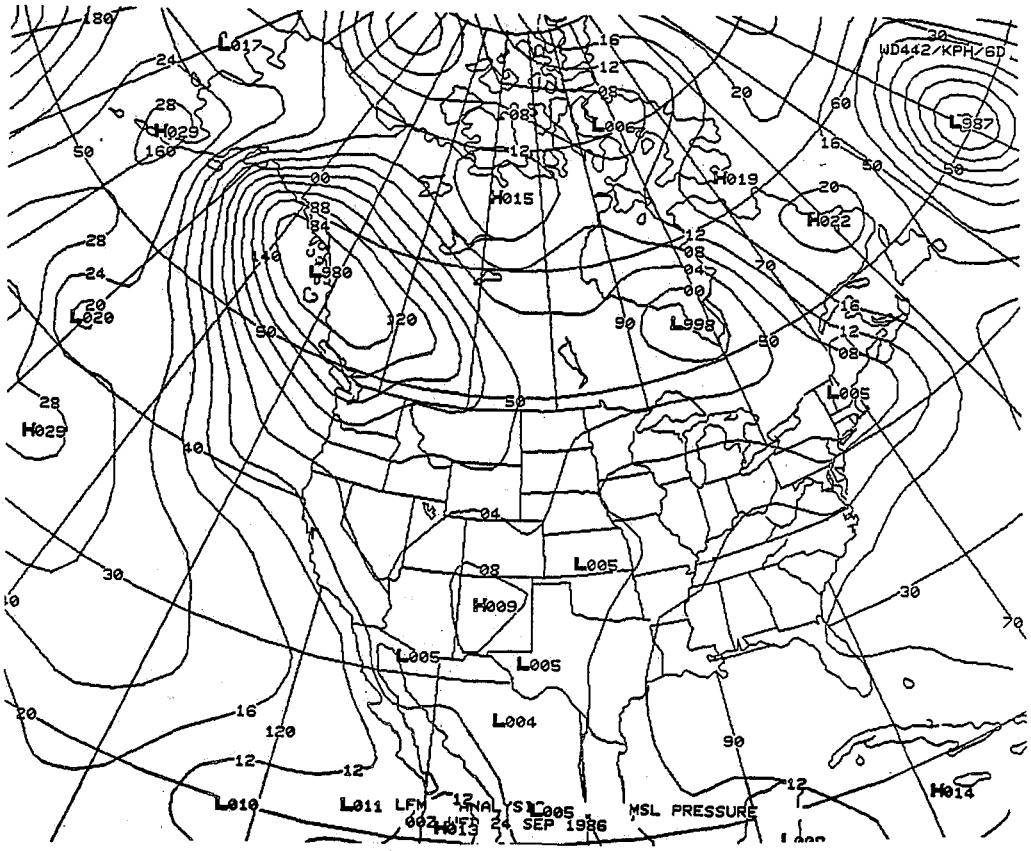

b

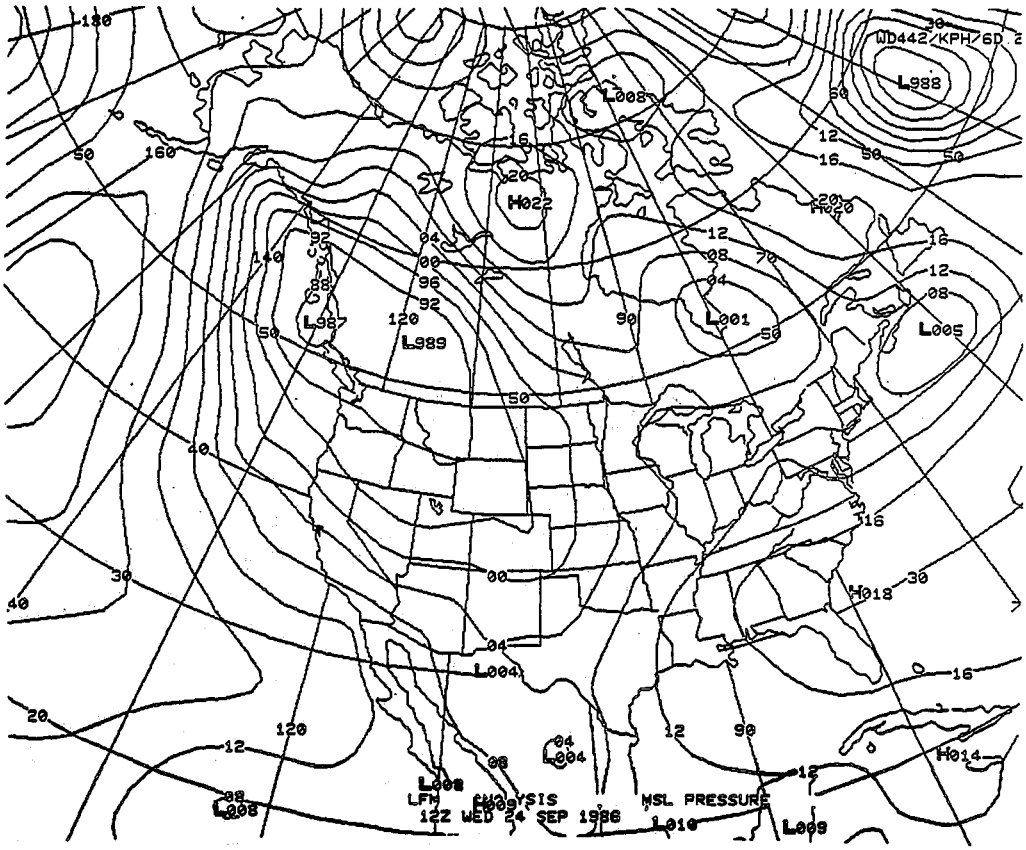

Fig. 6. LFM sea level pressure initial analyses for a) 0000 UTC September 24, b) 1200 UTC September 24, c) 0000 UTC September 25 and d) 1200 UTC September 25.

c

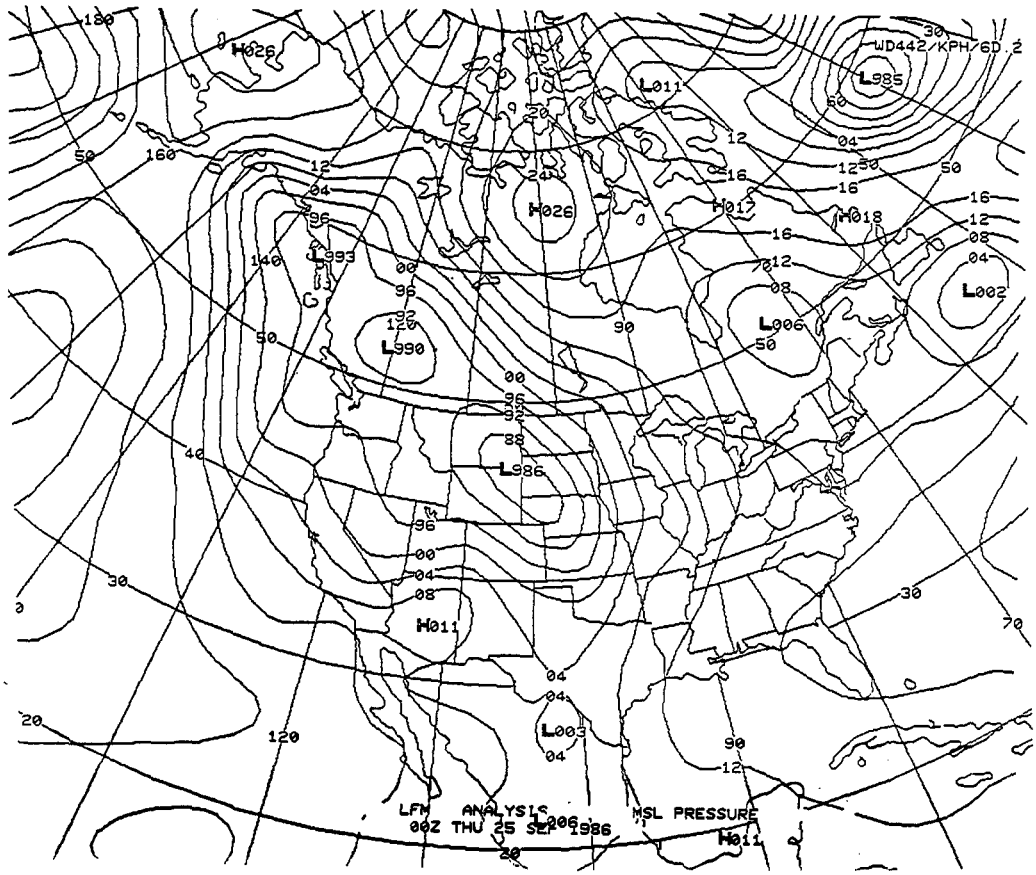
WD442/KPH/6D.2
H026
L011
L985
H026
H017
H018
L993
L002
L990
L006
L986
H011
L003
L006
H011
LFM ANALYSIS MSL PRESSURE
00Z THU 25 SEP 1986

d

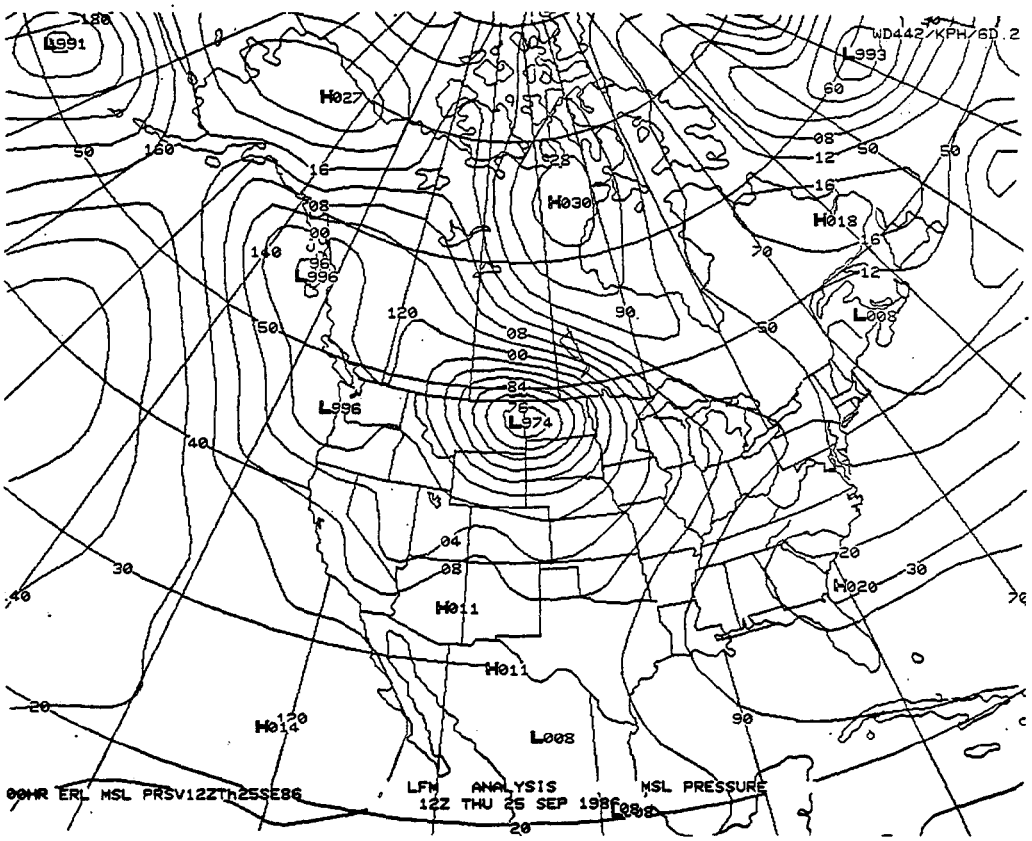
WD442/KPH/6D.2
L991
L993
H027
H030
H018
L996
L008
L996
L974
H011
H011
H020
H014
L008
00HR ERL MSL PRSV12ZTh25SE86
LFM ANALYSIS MSL PRESSURE
12Z THU 25 SEP 1986

Fig. 6 (cont.)

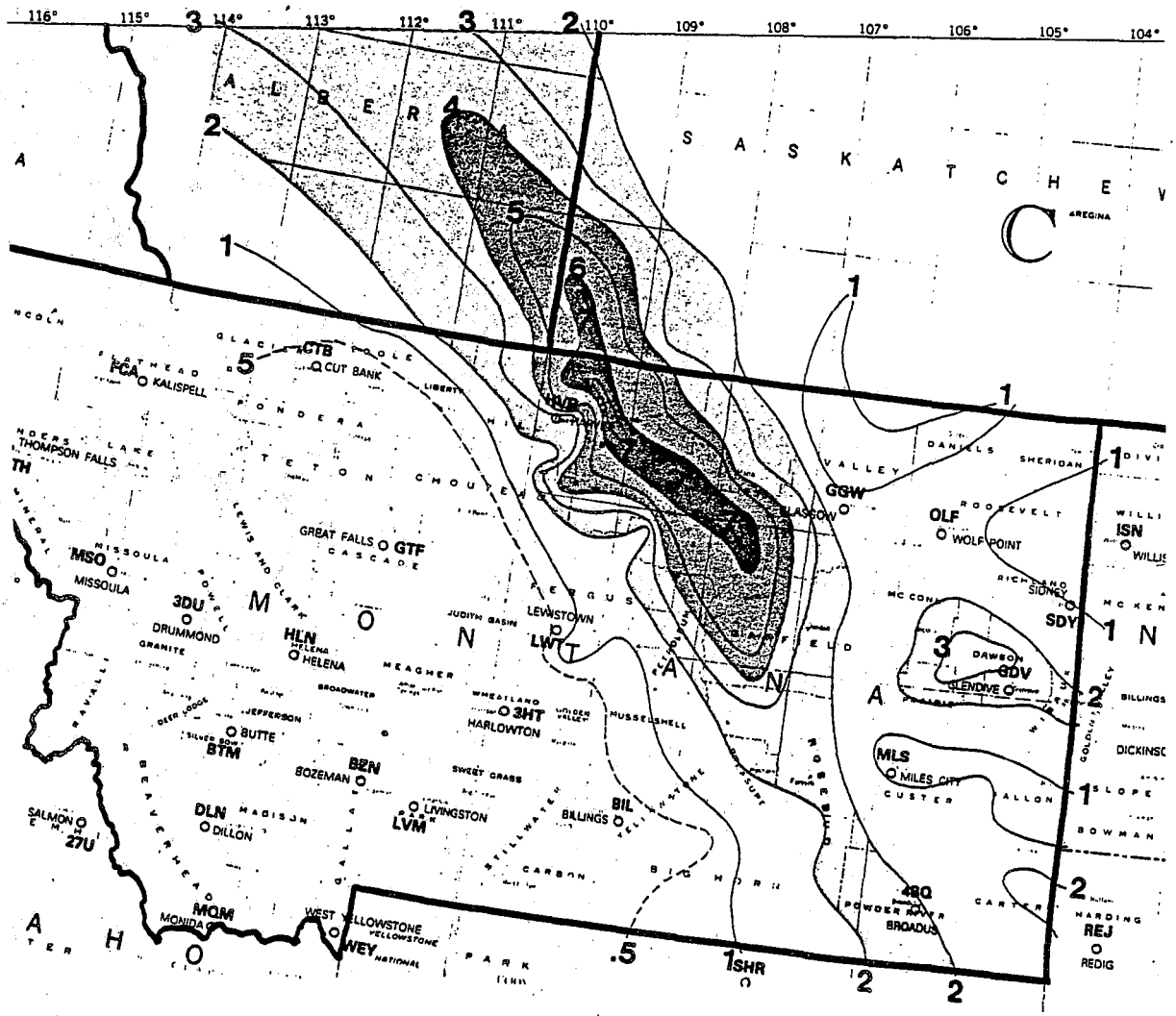

Fig. 7. Storm totals of precipitation in inches, September 24-26, 1986. Totals of 2-4 inches are shaded light, 4-6 inches are shaded medium and greater than 6 inches are shaded dark. The dashed line is the 1/2-inch contour. Precipitation began in southern Montana around 2100 UTC September 24, and ended in northern Montana around 0600 UTC September 26. Most fell between 0000 UTC and 1200 UTC September 25, including 5 inches in 6 hours at one automatic gauge in the Missouri River basin.

C. Rainfall Observations

Figure 7 shows the rainfall observed in Montana over the course of this storm, from late on the 24th through early on the 26th. Heaviest precipitation fell along an axis from about 60 miles southwest of Glasgow to 20 miles east of Havre. 2 inch rainfall totals extended both southeast and north of the state. The largest amounts were concentrated in north-central Montana and into southern Saskatchewan. Topography over the area shows some, but not a great deal of undulation (Figure 8). All elevations below 3000 feet above sea level are shaded, highlighting the Milk and Missouri River basins. Lack of significant topographical barriers seems to preclude a major topographical impact on the heavy precipitation amounts. Precipitation was first reported in southeastern Montana around 2100 UTC September 24. The low was deepening across western South Dakota and Nebraska at that time with a central pressure near 982 mb (Figure 9). By 0300 UTC September 25 (Figure 10), the rain had begun in northern Montana with the central pressure of the surface low dropping to near 974 mb at the Montana/Wyoming/South Dakota intersection. Heaviest rainfall from 0600 UTC to 1800 UTC was observed over the Missouri and Milk River watersheds (west of Glasgow and east of Havre). During this time, the surface low tracked northward to near the northern Montana/North Dakota border, had deepened to near 970 mb at 1200 UTC and filled to near 972 mb at 1800 UTC (Figures 11, 12).

The inverted trough extended along the heavy rain axis northwestward from the low during this period. The heavy rains apparently increased northwestward and decreased from the south along the inverted trough axis during this period. After 1200 UTC, the rains had diminished across the Missouri River basin. By 0900 UTC Medicine Hat, Alberta (YXH) was reporting moderate rainfall (the Havre report was missing). Both Havre and Medicine Hat then indicated moderate rainfall on the 3-hourly maps until 1800 UTC. The intensity had decreased to light rain at both sites at 2100 UTC and beyond.

D. Derived Fields

Perhaps one of the most important forcings involved in any developing system is the horizontal and vertical structure of convergence. Likewise, in a case such as this where very heavy amounts of precipitation fell, convergence patterns must exhibit strong signals in the horizontal flow fields to produce the required vertical motion field. Mesoscale convergence patterns were calculated at the surface, 850, 700, 500, 300 and 250 mb on 0000 UTC and 1200 UTC of the 25th, these times being just prior to and during the late stages of the heaviest rainfall across Montana, respectively. At 0000 UTC, the values shown are for 45N/106W - near the convergence centers

Fig. 8. Topography of Montana east of the continental divide. Shaded areas are below 3000 feet above sea level.

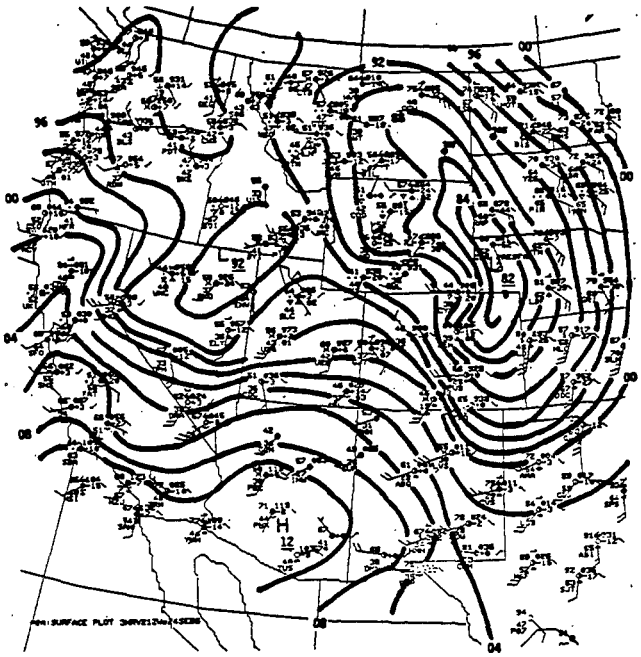

9

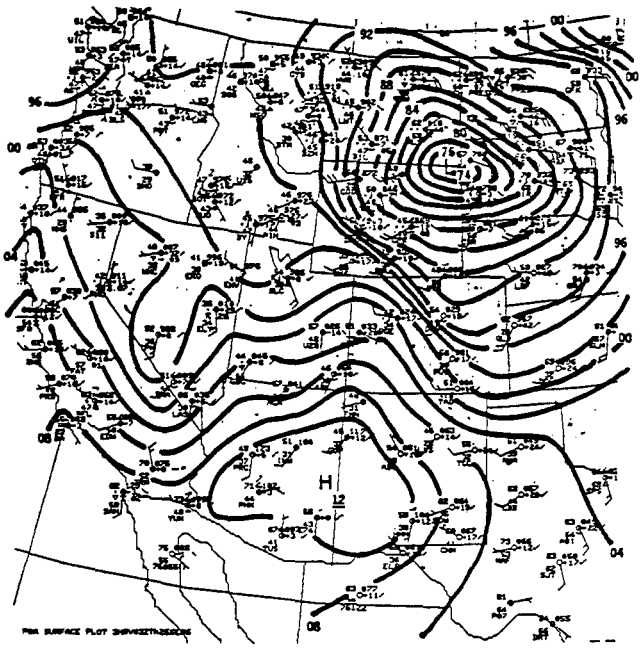

10

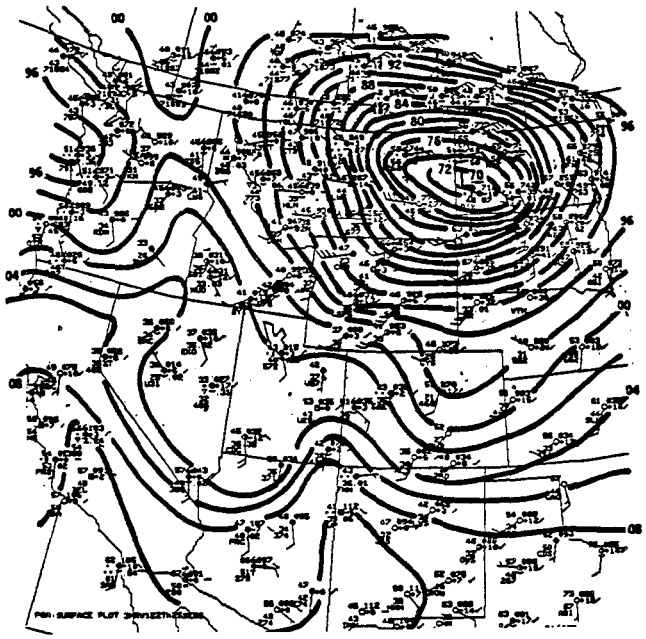

11

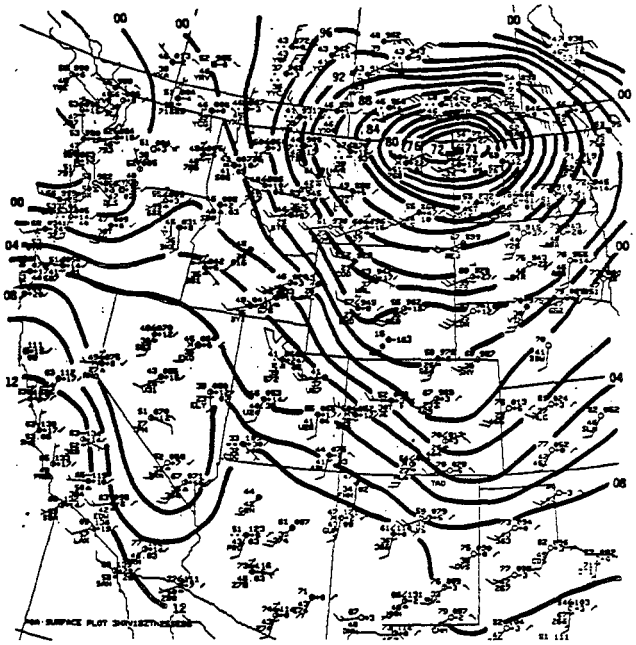

12

Fig. 9. Sea level pressure analysis valid 2100 UTC September 24. Contour interval 2 mb.

Fig. 10. As in Figure 9, except for 0300 UTC September 25.

Fig. 11. As in Figure 9, except for 1200 UTC September 25.

Fig. 12. As in Figure 9, except for 1800 UTC September 25.

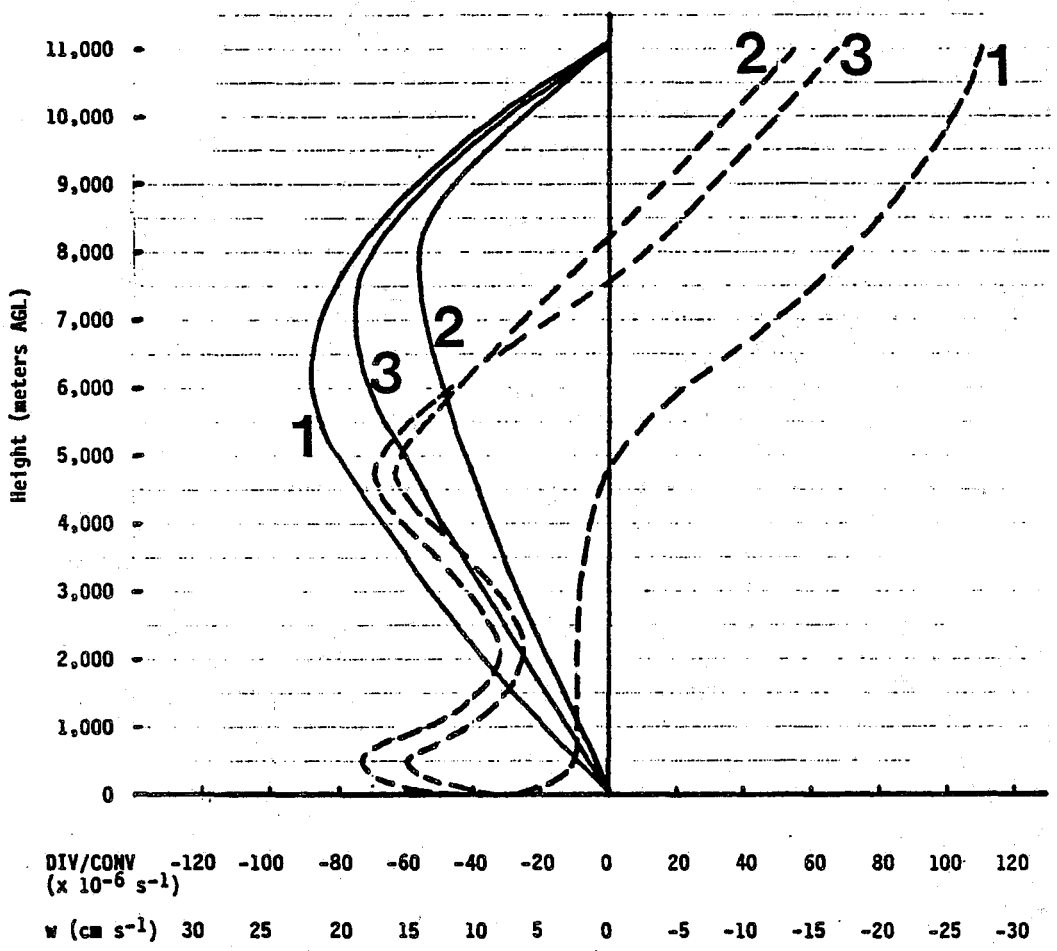

Fig. 13. Kinematic divergence (dashed) and vertical velocity profiles (solid). Lines numbered 1 correspond to 0000 UTC September 25 at 45N/106W, lines numbered 2 for 1200 UTC September 25 at 48.5N/108.5W and lines numbered 3 for slantwise parcel movement at 49N/108W near the surface to 48N/111W near the tropopause for 1200 UTC September 25. Vertical velocity assumes no net columnar divergence; constant linear correction method used for normalization. Divergence calculations based on a 1.2° longitude x 1.4° latitude grid; two smoothing passes made.

of action. At 1200 UTC, the values are for 48.5N/109W. The analysis was extrapolated to 200 mb, the location of the tropopause according to the nearby Glasgow soundings. These calculations are summarized by dashed lines 1 and 2 in Figure 13. One of the striking points in this analysis is that kinematic values show significant total columnar divergence through the layer at 0000 UTC. Not coincidentally, this was the time at which the surface pressure was deepening in southeastern Montana. At 1200 UTC, the convergent nature of the vertical layer indicates that the system is filling through northern Montana.

Figure 13 also shows the resultant vertical motion values at 0000 UTC and 1200 UTC. Vertical motion is calculated from the fixed lower surface, assuming mass continuity and no net total convergence or divergence in the column. Therefore, the change in vertical motion with height is directly related to integrated horizontal convergence over each individual layer. For our purposes, given only discrete observations, averaging convergence values at each level gives us the mean convergence over the layer which we multiply by the thickness of the layer. This value equals the change in vertical motion over the layer. (Since total divergence values did not equal 0, the constant correction method was used throughout the vertical column so that the vertical velocity was also 0 at the tropopause, thus satisfying the continuity equation).

There are two 1200 UTC profiles of divergence and vertical velocity shown in Figure 13. One assumes the purely upright profile of convergence/divergence couplets, as discussed earlier, at 48.5N/109W. The other is more realistic in that it follows the convergence or divergence axes to the southwest with height - sloping across the frontal zone more as a parcel would travel. This will be elaborated on later. The kinematic vertical motion profiles show values around 20 cm/s (approximately equal to 20 microbars/s - the value depicted on the standard operational vertical velocity prognoses). These values represent the maximum present over the area. It should be noted that they are representative of a 155.4 km x 91.2 km (14,172 km^2) area given that such was the grid spacing of the convergence calculations. While these are not impressive values when compared with those found within thunderstorm updrafts, on such a scale as this, they are significant vertical velocities. Analyses using tighter grid spacing (110 km x 76 km) yield results which are on the average about 30% larger, thus indicating vertical velocities of over 26 cm/s over an 8360 km^2 area. The series of convergence charts used are shown in Figures 14 and 15. Table 1 summarizes the values used for calculating the vertical velocities on Figure 13.

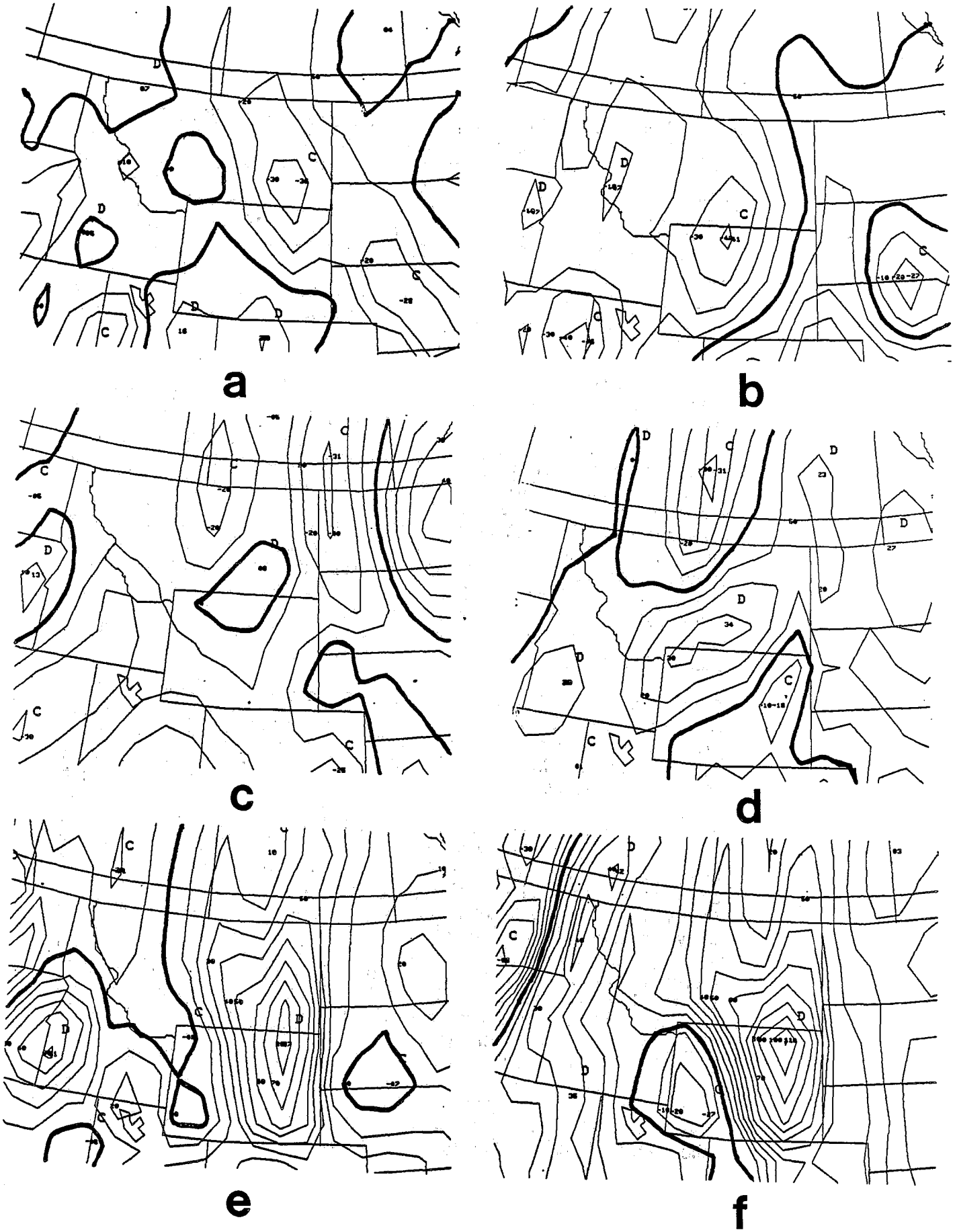

Fig. 14. Mesoanalysis of convergence at 0000 UTC September 25 at a) surface, b) 850 mb, c) 700 mb, d) 500 mb, e) 300 mb and f) 250 mb. Values based on 1.4° latitude x 1.2° longitude grid with 2 smoothing passes. Negative values indicate convergence, units are 10^{-6} sec^{-1} with a contour interval of 10. Heavy line is zero contour.

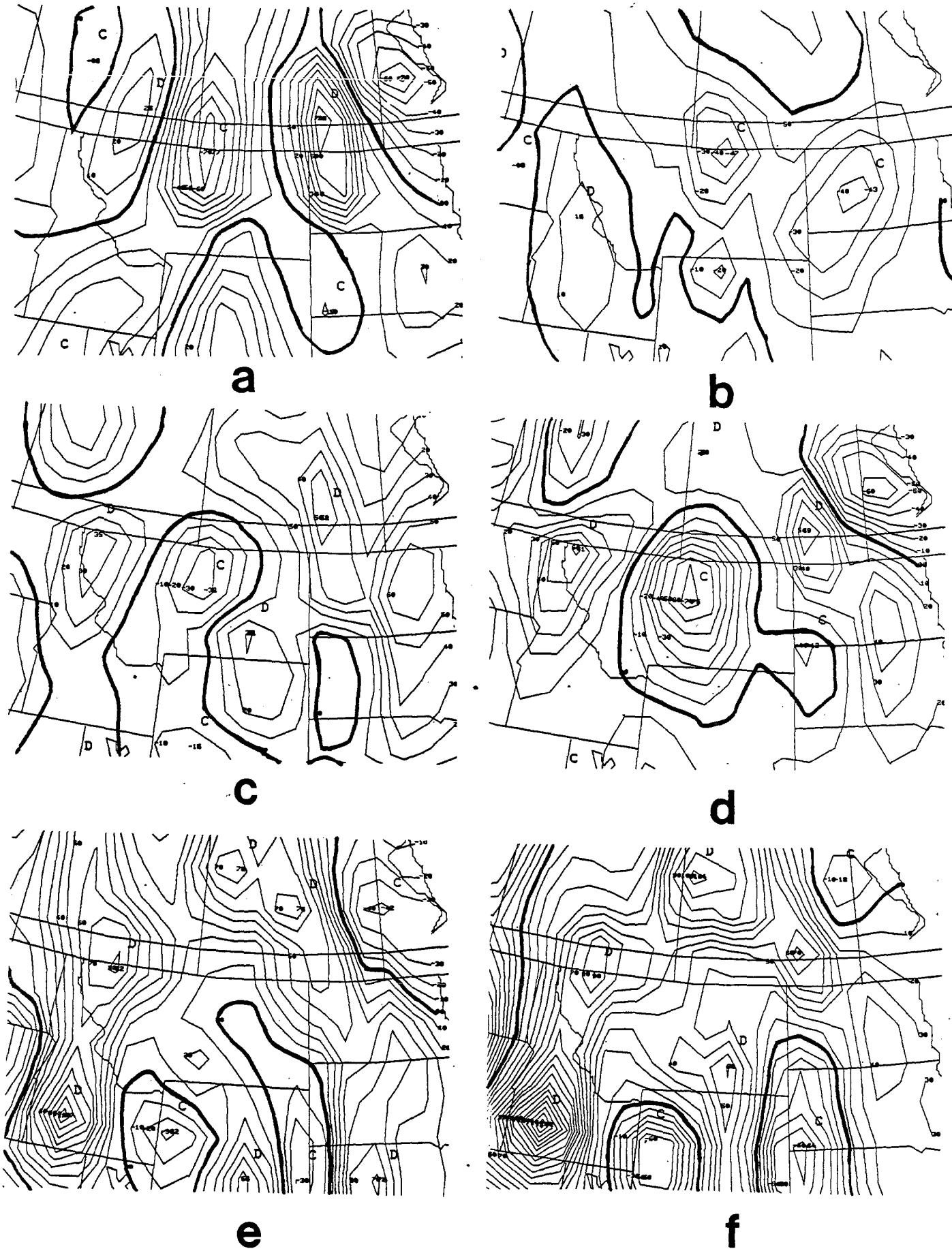

Fig. 15. As in Figure 14, except for 1200 UTC September 25.

level	layer	DIV(+)/CONV(-)			ht AGL (m)			layer thickness(m)			mean layer DIV(+)/CONV(-)		
		00Z	12Z-U	12Z-S	00Z	12Z-U	12Z-S	00Z	12Z-U	12Z-S	00Z	12Z-U	12Z-S
sfc		-30	-35	-47	0	0	0						
	1							500	500	500	-20	-47	-60
850		-10	-60	-73	500	500	500						
	2							1650	1600	1600	-10	-43	-52
700		-10	-26	-31	2150	2100	2100						
	3							2690	2700	2700	- 5	-45	-50
500		0	-64	-70	4840	4800	4800						
	4							0	3480	2800	0	-32	-35
LND		0	0	0	4840	8280	7600						
	5							3700	200	880	40	3	11
300		80	5	21	8540	8480	8480						
	6							1260	1250	1250	90	18	33
250		100	30	45	9800	9730	9730						
	7							1300	1270	1270	105	43	57
200		110	55	68	11100	11000	11000						

level	layer	layer dw (cm/s)			w (cm/s)			normalized w (cm/s)		
		00Z	12Z-U	12Z-S	00Z	12Z-U	12Z-S	00Z	12Z-U	12Z-S
sfc					0.00	0.00	0.00	0.00	0.00	0.00
	1	1.00	2.35	3.00						
850					1.00	2.35	3.00	2.61	1.22	1.94
	2	1.65	6.88	8.32						
700					2.65	9.23	11.32	9.58	4.51	6.88
	3	1.35	12.15	13.50						
500					4.00	21.38	24.82	19.61	10.58	14.66
	4	0.00	11.14	9.80						
LND					4.00	32.52	34.62	*21.94	13.89	18.54
	5	-14.80	-0.06	-0.97						
300					-10.80	32.46	33.65	16.65	13.38	15.70
	6	-11.34	-2.25	-4.13						
250					-22.14	30.21	29.52	9.60	8.32	8.91
	7	-13.65	-5.46	-6.24						
200					-35.79	24.75	23.28	0.00	0.00	0.00

* At 6300 meters due to implied normalized change in vertical divergence structure

Table 1. Summary of values used in calculating normalized vertical velocities in Figure 13. 12Z-U indicates values for upright calculations; 12Z-S is for slantwise parcel trajectory. Normalized w based on the equation $w = w_{200} - (ht/ht_{200} * w_{200})$. Divergence values interpolated to the level of non-divergence (LND) and extrapolated to 200 mb (from 250 mb); 200 mb was approximately the tropopause based on sounding data. Divergence in units of 10^{-6} sec^{-1}. Layer dw determined by layer thickness * mean layer divergence.

II. MODEL PERFORMANCE

The Limited-area Fine Mesh (LFM) model and Nested Grid Model (NGM) 36 and 48-hour forecasts of 500 mb height and vorticity and surface pressure valid at 1200 UTC September 25 are shown in Figure 16. The 500 mb short wave was forecast to be somewhere between the western Dakotas to the Canadian border of North Dakota on all of these prognoses. The timing of the system appeared to be handled rather well in the day 2 forecast as the actual location of the vorticity center was in western North Dakota (Figure 5d). The models had a much harder time resolving the magnitude of surface development and its location, and the related development of the system aloft.

The LFM was consistent between these two model runs by forecasting central surface pressures near 990 mb at the central North and South Dakota border. The NGM was markedly different from the LFM at the surface, though also consistent between the two runs. It placed a surface low center well north of Montana with a trough extending southeastward toward the northern North Dakota border. Neither of these runs suggested the development of a 974 mb low or the strong low level convergence that verified on 1200 UTC September 25 (Figure 6d).

Figure 17 shows the 12 and 24-hour LFM and NGM forecasts of 500 mb height and vorticity and surface pressure valid at 1200 UTC September 25. Both models tended toward verifying truth, as the NGM 12 and 24-hour forecasts indicated the development of a significant (970 to 972 mb) surface low in northeastern Montana. Likewise, and perhaps as a result, the NGM developed the upper level system much stronger than the LFM, which forecast a surface low center between 983 to 985 mb in western North Dakota on the two runs. Both models had the correct trend (that is, toward greater low-level convergence on the shorter range runs), though the NGM more strongly suggested what actually occurred.

Quite obviously, the forecaster would have been hard pressed to forecast the extreme amounts of precipitation over north-central Montana based on either model run at 36 or 48 hours. The first good forecast of surface and upper level features was the NGM 24-hour guidance. However, since no previous NGM or LFM run was anywhere near as strong on this short wave, it would not be surprising for the forecaster to reject the best of the guidance as being out of line. Though the NGM was realistic in the development of the system in northeastern Montana, 24-hour QPF between 0000 UTC September 25 and 0000 UTC September 26 from the most accurate (12-hour) run (initialized 0000 UTC September 25) indicated maximum amounts of less than 2-1/2 inches (Figure 18) at any given model grid point (each representing approximately 7300 km^2). Since these values represent the mean over this area, it is possible that the maximum is a smoothed representation of localized 4" rainfalls within a particular grid box. Given that there were reports of over 5

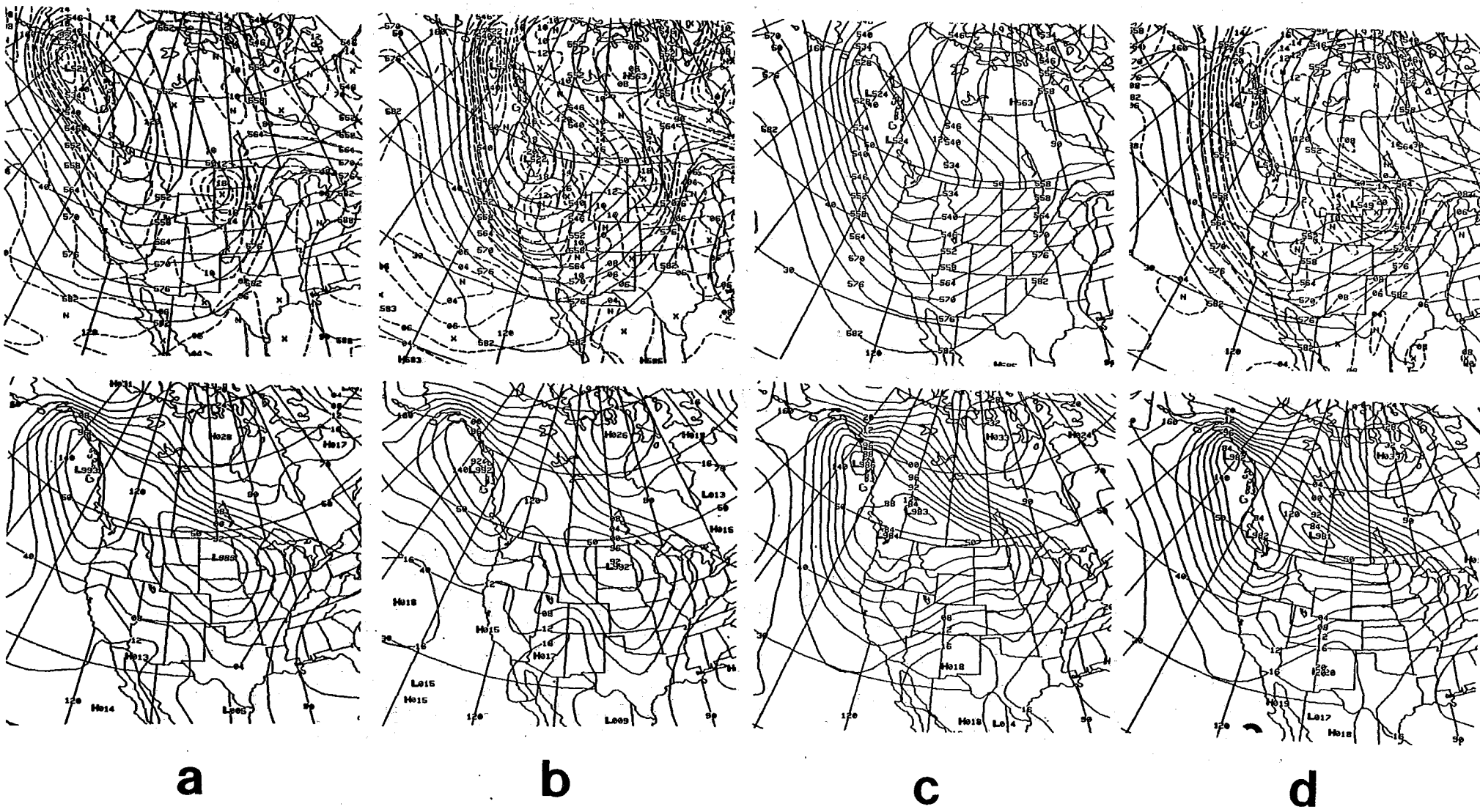

Fig. 16. Forecast 500 mb heights and vorticity, and sea level pressure valid 1200 UTC September 25 from a) LFM 36-hour run, b) LFM 48-hour run, c) NGM 36-hour run and d) NGM 48-hour run.

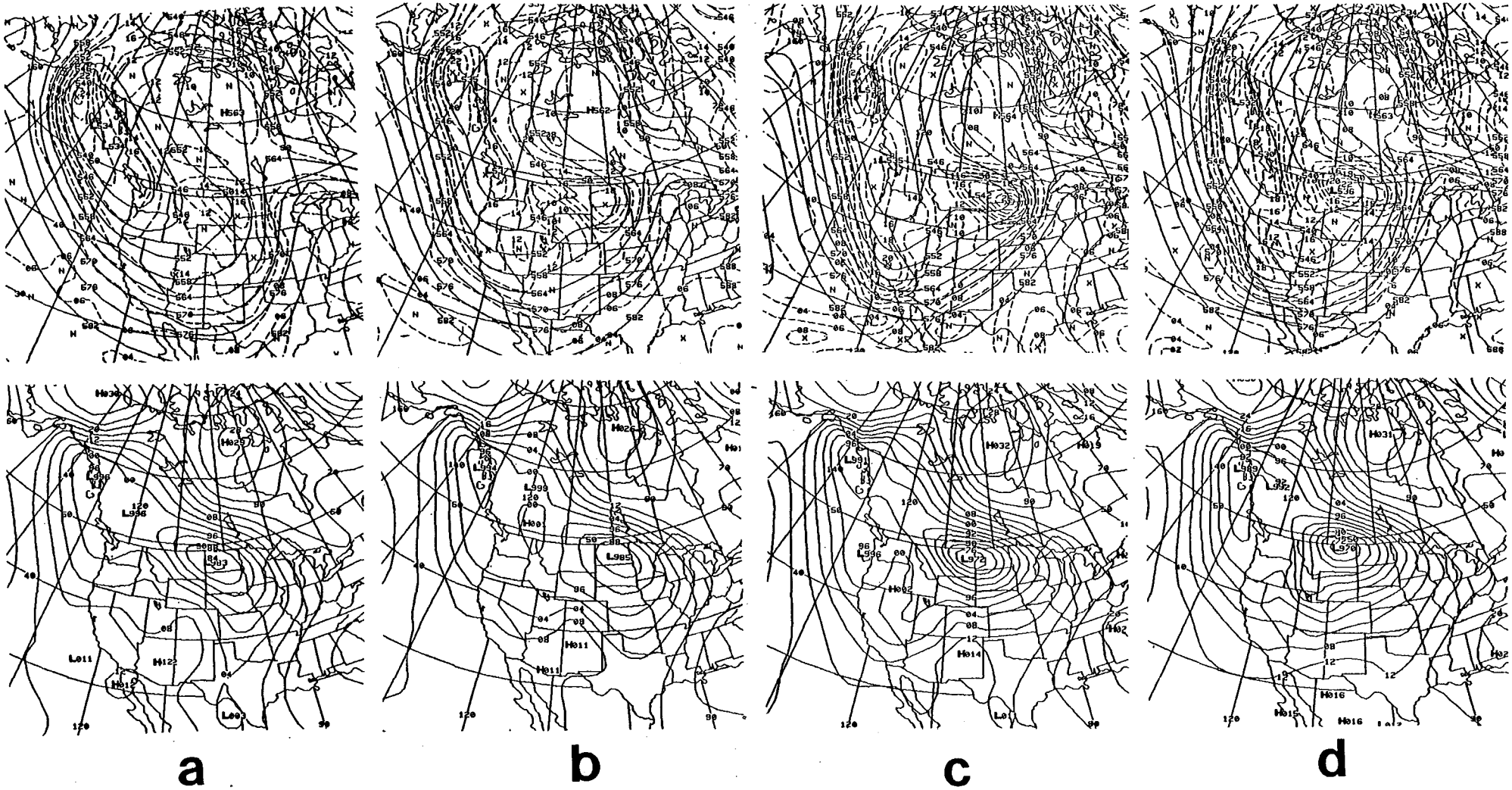

Fig. 17. As in Figure 16, except from a) LFM 12-hour run, b) LFM 24-hour run, c) NGM 12-hour run and d) NGM 24-hour run.

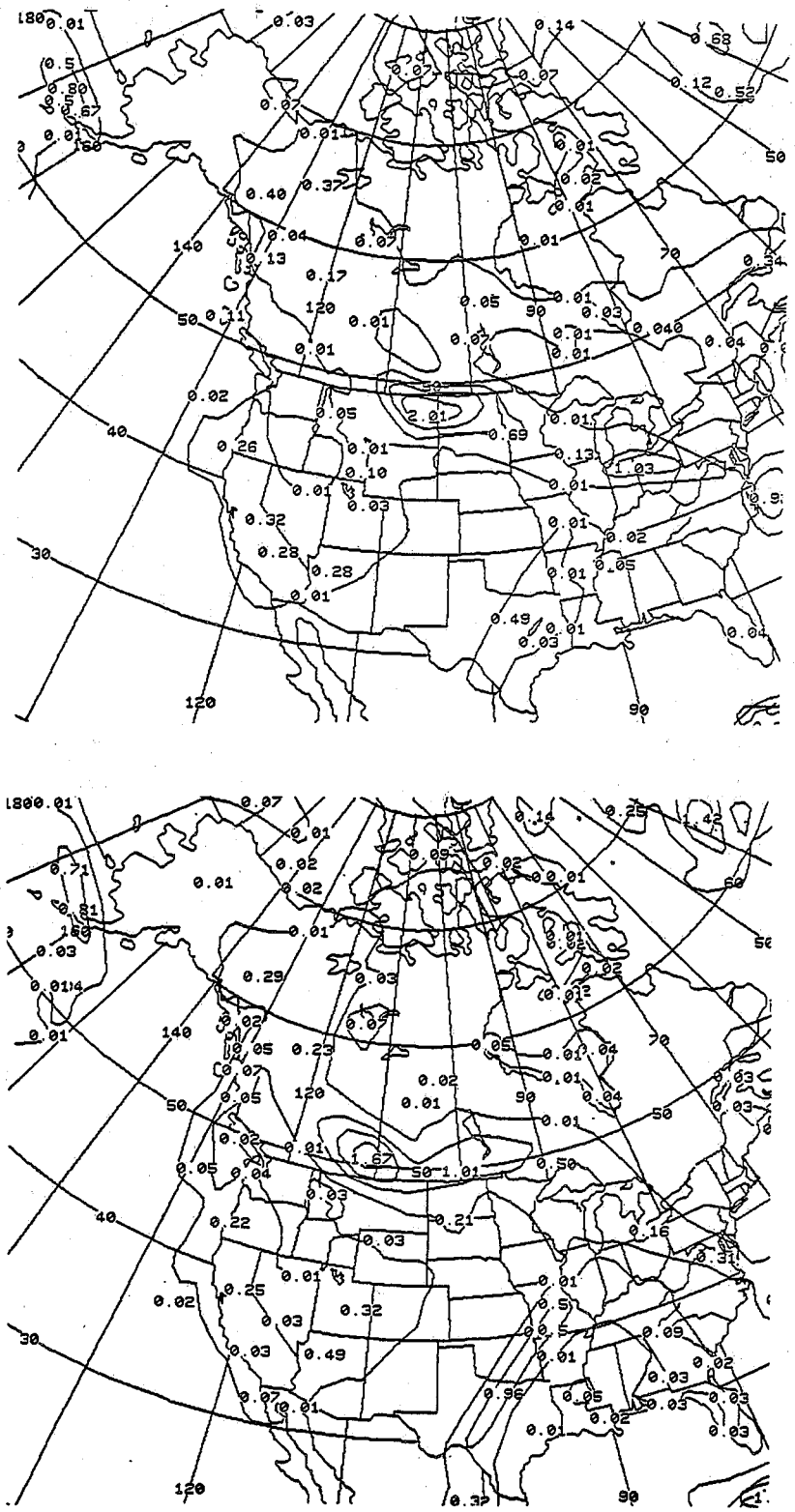

Fig. 18. NGM QPF forecasts from the 0000 UTC September 25 run - a) 12-hour forecast valid 1200 UTC September 25, b) 24-hour for the 12 hours ending 0000 UTC September 26.

inches over twice that area, however, the short-term NGM runs, even with realistic surface development, significantly underestimated the precipitation over the heavy rain area. As a result, even if the forecaster bought the system development of the NGM, the amounts of precipitation that fell would probably still have been a surprise.

When confronted with the choice between the LFM and NGM model runs at 12 and 24-hours, the field forecaster is faced with a decision-which model run to choose. This decision brings up two questions: 1) is there a difference between the two models physically that would favor one over the other, and 2) if so, have these physical differences been evident in recent model performances?

There are many differences between the LFM and the NGM with respect to the way they handle developing systems. Perhaps one of the most important differences between the two models in this case is the way surface drag over the mountains is prescribed. As described in Western Region Technical Attachment (WRTA) 86-30:

> "The surface drag coefficient in the NGM is determined by the surface roughness length... defined mostly by vegetation type. The... drag coefficient developed by G. Cressman... varied mostly in response to height of the ground. It (the Cressman coefficient) very likely gave larger frictional effects over the Rockies than does the NGM formulation. The LFM still uses the Cressman formulation of the drag coefficient."

Therefore, the greater frictional effects of the LFM compared to the NGM may have made an impact on the difference between the central pressure of the two model forecasts.

A second difference may have been due to the grid spacing used by the models. The NGM may have more accurately captured smaller-scale forcings (or maintained their intensity) better than the LFM, thus achieving greater surface development than the LFM. There are undoubtedly other physical differences between the models that played a role, especially those that are important when considering rapidly developing systems. These, however, are two of the most obvious differences that might influence what the sea level pressure fields looked like.

Finally, the NGM surface fields tend to handle gradients and fronts more precisely than do the LFM fields, probably due to greater vertical resolution in the lower levels. This may have been an important difference between the two models in the 12-24 hour forecasts. Because of the greater low-level vertical resolution, the NGM may have developed the system more strongly than the LFM due to more accurate handling of the large amounts of latent heat release in the lower troposphere. As discussed in the next section, latent heat release is an important feature of rapidly developing cyclones.

The second question asks how the models have been performing, attempting to pin down which of the models have been physically handling the details of the large scale flow pattern better, given the recent track record. In this instance, the NGM had been performing rather poorly by overdeveloping several weaker disturbances near Montana in the previous week or so. A similar system to these erroneous NGM forecasts, though it occurred after the case presented here, was discussed in WRTA 86-30, and exemplifies the problems the model had been having. With this in mind, it would have been that much more difficult to accept the NGM "bomb" being forecast on the 1200 UTC September 24 run.

The major difference between the erroneous NGM developments of the previous week and the good forecast in this case is that the erroneous developments showed up in day 2 of the model run (and thus could have originated in the data-poor east Pacific) whereas, in this case, the strong development occurred in day 1 of the run.

III. DISCUSSION

Up to this point, we have mainly looked at the observations and model performance in this case study. We have noted that there was fairly strong kinematic vertical motion over much of eastern Montana at some point during this storm. The strongest kinematic vertical motion apparently tracked from the southeastern part of the state to near Havre between 0000 UTC and 1200 UTC September 25. We reviewed the performance of the short-term models. Even the NGM runs which captured the surface development fairly well missed the intensity of the heavy rainfall. We have noted that while the rainfall was heavy over a large area, the heaviest amounts were oriented along a relatively narrow band, for the most part parallel to the trough axis from the lower layers through the mid-levels during the heavy rain period. This section will try to apply what we have observed and derived to an examination of some physical processes that may have been important in creating this flooding event.

A. Surface Low Development

The processes which most likely aided the initial cyclone development seem to be fairly basic. Evidence for lee side troughing in eastern Colorado and Wyoming exists at the surface during the afternoon of the 24th (Figures 6b,c). As the closed low and vorticity center rotated northeastward from western Arizona to eastern Colorado and Wyoming during the afternoon, strong PVA existed over the region of development (Figures 5b,c).

Subsequent strong development of this system was more than basic; technically, it was a "bomb". The requirement of this classification is a deepening of the central pressure by at least 24 mb per 24 hours, which is approximately how much this

system deepened between 1200 UTC September 24 and 25. While bombs are typically considered oceanic phenomena, this storm had one of the most important characteristics needed, that being a substantial low-level moisture supply. This moisture supply, in concert with the release of a large amount of latent heat at low levels, acts to destabilize the atmosphere to such a point that the vertical motion, traditionally thought of as the "braking term" to cyclone development, no longer retards but actually contributes **positively** to the surface development. In this regard, the fact that remnants of Hurricane Newton had moved into the Great Plains region over the previous couple of days may have impacted the system development. Surface dew points through Kansas, Nebraska and South Dakota were generally over 60°F while the system developed in the western portion of these states. That the moisture existed at low levels is also important because with it, the release of latent heat will generally occur at lower levels which destabilizes the atmosphere more than latent heat release at mid or upper levels would.

B. Moisture, Baroclinicity and Frontogenesis

Associated with this system was a strong baroclinic zone evident at 700 mb at both 0000 UTC and 1200 UTC September 24 (Figure 19). Amplification of a wave along a strong baroclinic zone is not uncommon if a perturbation is introduced into the flow.

Moisture again is an important consideration here since baroclinicity essentially describes the condition where surfaces of constant pressure and density do not coincide. In most cases, we simply look for the strong temperature gradient on a constant pressure surface. This, we reason, shows the area of greatest density discontinuity and, likewise, the area of strongest baroclinicity and potential system development. We must, however, include moisture in the thermal structure such that we look at the **virtual** temperature gradient, which gives a truer representation of the density discontinuity.

Calculations at the surface and 700 mb, from eastern Colorado to western South Dakota (Table 2) show that in the region of development, the existence of the moisture gradient across the thermal gradient increased the baroclinicity by over 33% in some areas. It can now be postulated that the reason the regional models may have erred so significantly on the 36 and 48-hour forecasts in this case was because they did not incorporate the influx of Newton moisture into the Great Plains very well. Once the moisture was in the plains - on 1200 UTC September 24 - the NGM began to develop the system strongly. The LFM also trended in the right direction.

Latent heat release, besides being important in the surface

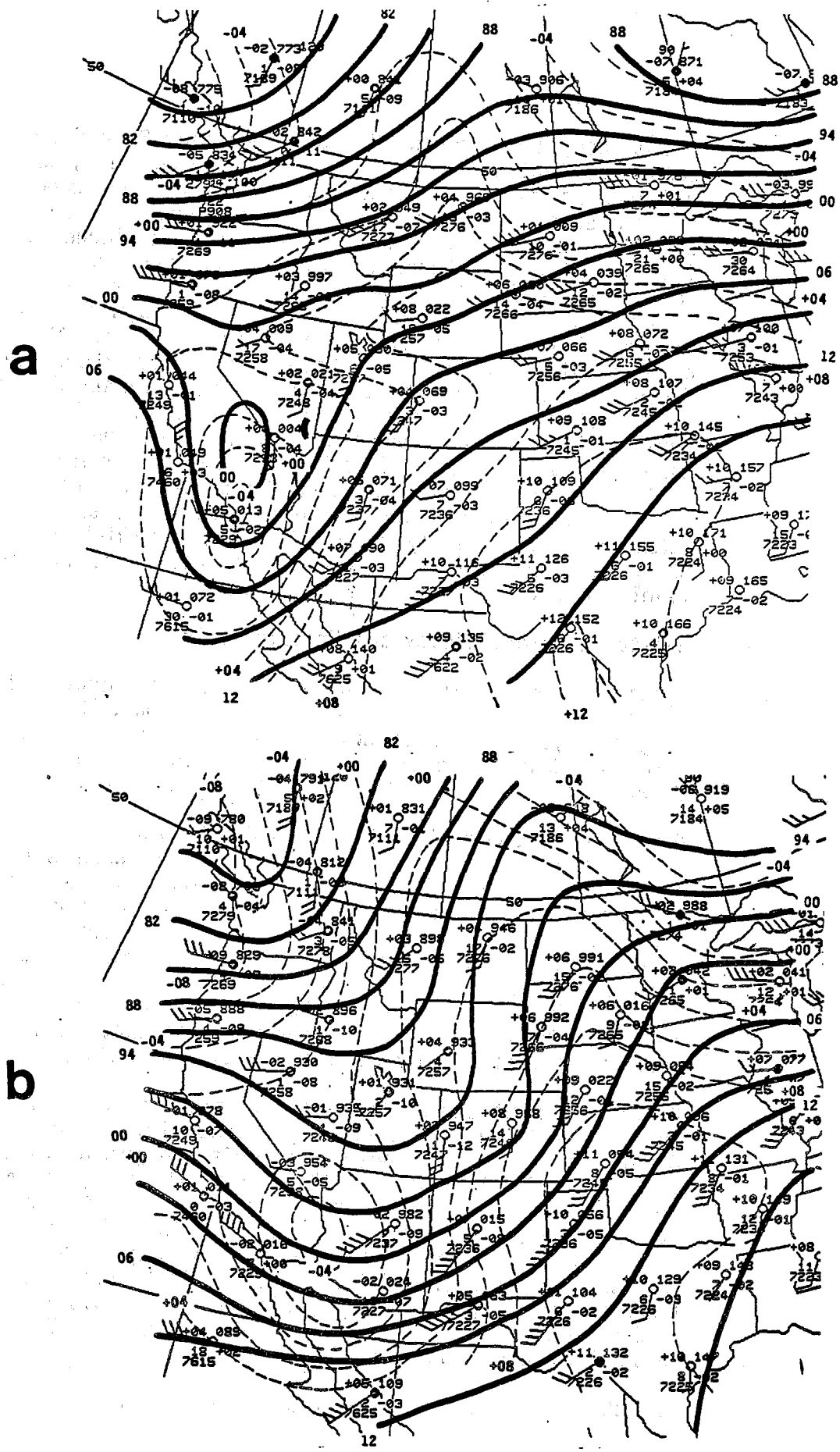

Fig. 19. 700 mb height and temperature analysis for a) 0000 UTC and b) 1200 UTC September 24. Height (solid) contours every 30 meters, temperature (dashed) contours every 2°C.

Surface 1800 UTC 9/24/86			
	T	T_d	T_v
PUB	19.5	0.0	20.3
DDC	25.0	18.0	27.7
	T = 5.5°C		
	T_v = 7.4°C		
% increase of gradient	34.5%		

700 mb 0000 UTC 9/25/86			
	T	T_d	T_v
DEN	3.0	-13.0	3.3
RAP	8.0	10.0	10.0
	T = 5.0°C		
	T_v = 6.7°C		
% increase of gradient	34.0%		

All temperatures are in °C.

Table 2. Temperature, dew point temperature and virtual temperature for Pueblo (PUB) and Dodge City (DDC) at 1800 UTC September 24, and Denver (DEN) and Rapid City (RAP) at 0000 UTC September 25. Temperature difference, virtual temperature difference and percentage increase of difference due to moisture is shown.

system development due to decreased vertical stability, also played a frontogenetical role in this case. Evident most clearly on the 1201 UTC satellite picture from September 24 (Figure 4b) is the convection on the warm side of the baroclinic zone and the lack of the same over eastern Colorado. The main source of the moisture associated with this convection was Hurricane Newton. That latent heat was released in the warm air and not in the cooler air strengthened the thermal gradient and baroclinicity in the lower layers of the atmosphere.

C. Frontogenesis and the Secondary Circulation

If frontogenesis exists across an area (if the density gradient increases with time), ageostrophic circulations are required to adjust the atmosphere. This adjustment is needed because when the density gradient increases, the thermal wind must also increase. But as the thermal wind increases, so must the actual wind, if it is to remain in geostrophic balance. Increasing the horizontal wind due to an increase in the thermal wind is accomplished through the secondary circulation, with positive ageostrophic vertical motions on the warm (less dense) side and subsidence on the cooler (more dense) side of the baroclinic zone. The horizontal flow of the secondary circulation, after being turned by the coriolis force, increases the wind above the intensifying baroclinic zone.

We may also look at this adjustment process through ageostrophic circulations from the point of view of Hoskins and Bretherton (1972), who point out that ageostrophic motions become increasingly important as relative vorticity is no longer small when compared to the coriolis parameter. Recall that relative vorticity is considered negligible, compared to the coriolis parameter within the quasi-geostrophic framework. As the relative vorticity increases, it is no longer negligible and the ageostrophic secondary circulations no longer can be considered as simple dynamical necessities to keep vorticity changes geostrophic and temperature changes hydrostatic within a synoptic scale system. Calculations of surface relative vorticity at 1200 UTC September 25 (Figure 20) show values upwards of 3×10^{-5} sec^{-1} extending northwestward into north-central Montana. At 500 mb, this value increases to 8×10^{-5} sec^{-1} on the LFM (Figure 5d). Obviously, these values are not negligible compared to the coriolis parameter and the ageostrophic circulations must be considered as a significant enhancement to the geostrophic flow field.

Additionally, Hoskins and Bretherton show that the ageostrophic circulation produces the tilt of the front and upgliding motion up the slope. This correlates well with the observations in this case, as the convergence/ divergence axes slope with height, probably with the frontal zone, in north-central Montana at 1200 UTC September 25 (see Figure 15).

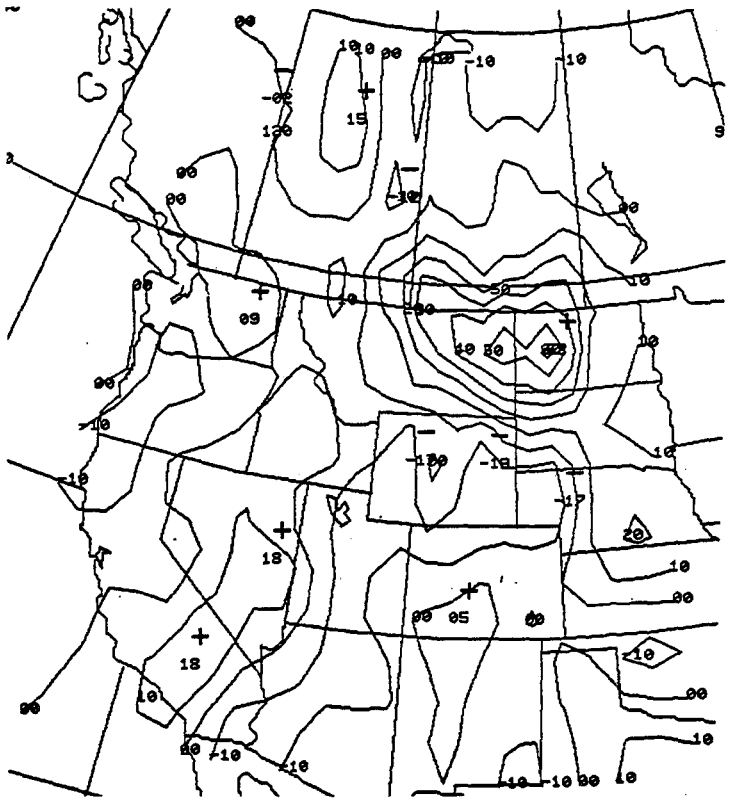

Fig. 20. Mesoanalysis of surface vorticity for 1200 UTC September 25, based on 1.4° latitude x 1.2° longitude grid; 2 smoothing passes made.

The secondary circulations described in the preceding paragraphs, including the ageostrophic vertical and horizontal flow fields, have been related to the deformation zone process of frontogenesis which can produce clouds and precipitation as discussed in WRTA 86-15. Here, we are applying the same frontogenetical concepts across the increasing moisture gradient in northern Montana. Figure 21 shows the progression of precipitable water values between 1200 UTC September 24 and 25. Intensification of the baroclinic zone due to vertically integrated moisture content is obvious across northern Montana as moisture from Hurricane Newton is advected across northeastern Montana from the Midwest. Westerly winds on the back side of the trough had cut off some of the moisture supply over the southern and western portions of Montana shortly after 0000 UTC September 25, which helped to intensify the moisture discontinuity. The difference in the vertical wind profiles across the frontal boundary shows up rather well on the Great Falls and Glasgow soundings from 1200 UTC September 25, shown in Figure 22.

D. Slantwise Convection and Symmetric Instability

The Glasgow sounding in Figure 22 is quite moist from the surface to 450 mb, typical of heavy rain soundings, and supportive of the widespread area of observed rainfall over 2 inches. The characteristic differences between heavy rain soundings and other severe weather soundings are the absence of dry air at mid levels and the lack of significant speed or directional shear in the vertical.

Though the heaviest precipitation covered a fairly large area in this case, it still had a linear orientation along the trough/convergence axis and showed amounts that were well above the surrounding areas of more general precipitation. This linear orientation suggests that some organized banding of convection may have existed that was not simply forced by the local structure of vertically integrated convergence.

It is in light of this evidence that we consider slantwise convection (due to symmetric instability) as a possibly important process in producing this very heavy band of precipitation. Evidence supporting this possibility includes the stability indices of the Glasgow and Great Falls soundings - both the Showalter and Lifted - all of which were slightly positive. This is not an uncommon observation in cases of slantwise convection, since generally speaking, unstable atmospheres would more easily give rise to upright convection. Stable atmospheres on the other hand, have greater difficulty producing upright convection.

A second important criteria for symmetric instability is the atmosphere's level of stability with respect to horizontal displacements, or it's inertial stability. For slantwise

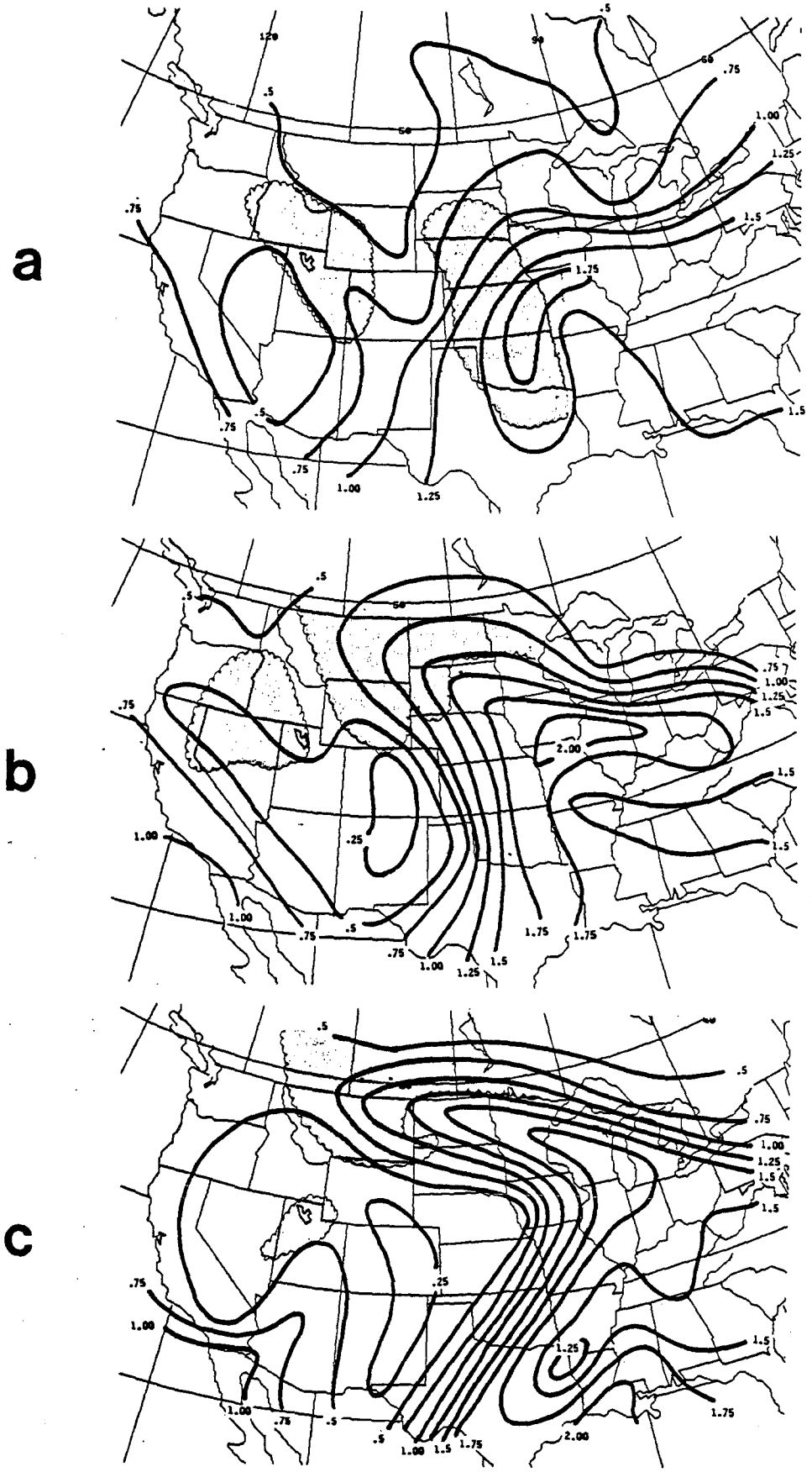

Fig. 21. Vertically integrated precipitable water (solid) and cloudiness (hatching) for a) 1200 UTC September 24, b) 0000 UTC September 25 and c) 1200 UTC September 25. Contour interval .25 inches.

a

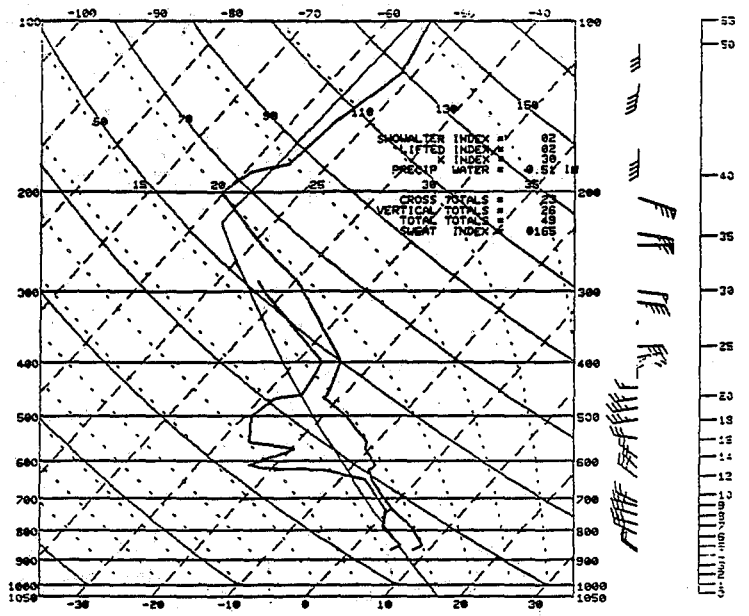

GTF 12Z 9/25/86

b

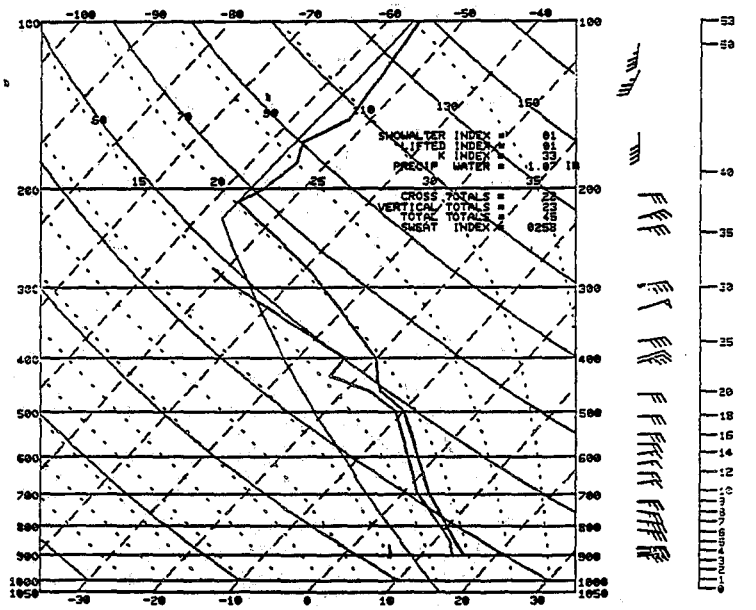

GGW 12Z 9/25/86

Fig. 22. a) Great Falls (GTF) and b) Glasgow (GGW) radiosonde observations from 1200 UTC September 25.

convection to occur, the atmosphere must not only be weakly stable in the vertical, but must also have sufficiently weak inertial stability to support positive horizontal buoyancy. From the 1200 UTC soundings in Figure 22, it is apparent that the upper level jet (200-300 mb) is nearer Great Falls than Glasgow. The concurrent 250 mb plot (Figure 23) shows that north-central Montana is under anticyclonic shear, yielding the situation whereby horizontal stability is weak, thus supporting this requirement for weak symmetric stability.

We have noted earlier the sloping nature of the convergence axes with height across northern Montana. We have also suggested mechanisms which would have enhanced the flow field across this implied sloping frontal axis. If symmetric instability exists, parcel displacement along the frontal axis may be oriented in such a manner that the parcels become positively buoyant, even in a statically and inertially stable environment. This novel and not-so-straightforward concept is explained most clearly by Sanders and Bosart (1985), following the theory developed mathematically by Emanuel (1983b). Emanuel (1985) has also shown that the region of ageostrophic ascent may become intense and concentrated in a relatively narrow band in the ascent along the sloping frontal boundary. This concentrated band of ascent may exist if the potential vorticity (the absolute vorticity times the change of potential temperature with respect to pressure) becomes very small in the warm air (due mainly to a pseudo-adiabatic lapse rate as applied to this case) and is **not small** in the region of downward motion, as is the case when such regions are unsaturated. Questions have been raised, however, as to whether symmetric instability-produced bands of intense ascent increase the total precipitation over the area upon which its influence is felt, or if it simply redistributes the precipitation into strong bands. Current research projects are focussing on this question.

The whole concept of symmetric instability can be viewed as being analogous to upright convection. The difference is that instead of assessing stability by forcing a parcel vertically, stability is determined by forcing the parcel both vertically and horizontally. The angle of forcing is taken to be along a surface of constant momentum M, as defined by Emanuel (1983b), with $M = v + fx$, where f is the coriolis parameter. If there exist locations where, following an M surface upward, the equivalent potential temperature (θ_e) decreases, instability exists. Much the same, if a parcel travels a slantwise path such that θ_e does not increase and M does not decrease, that parcel has encountered symmetric instability and is unstable, both vertically and horizontally, along that path, so long as such conditions exist.

To assess the possible existence of symmetric instability in this case, Figure 24 has plotted on it the θ_e and M fields

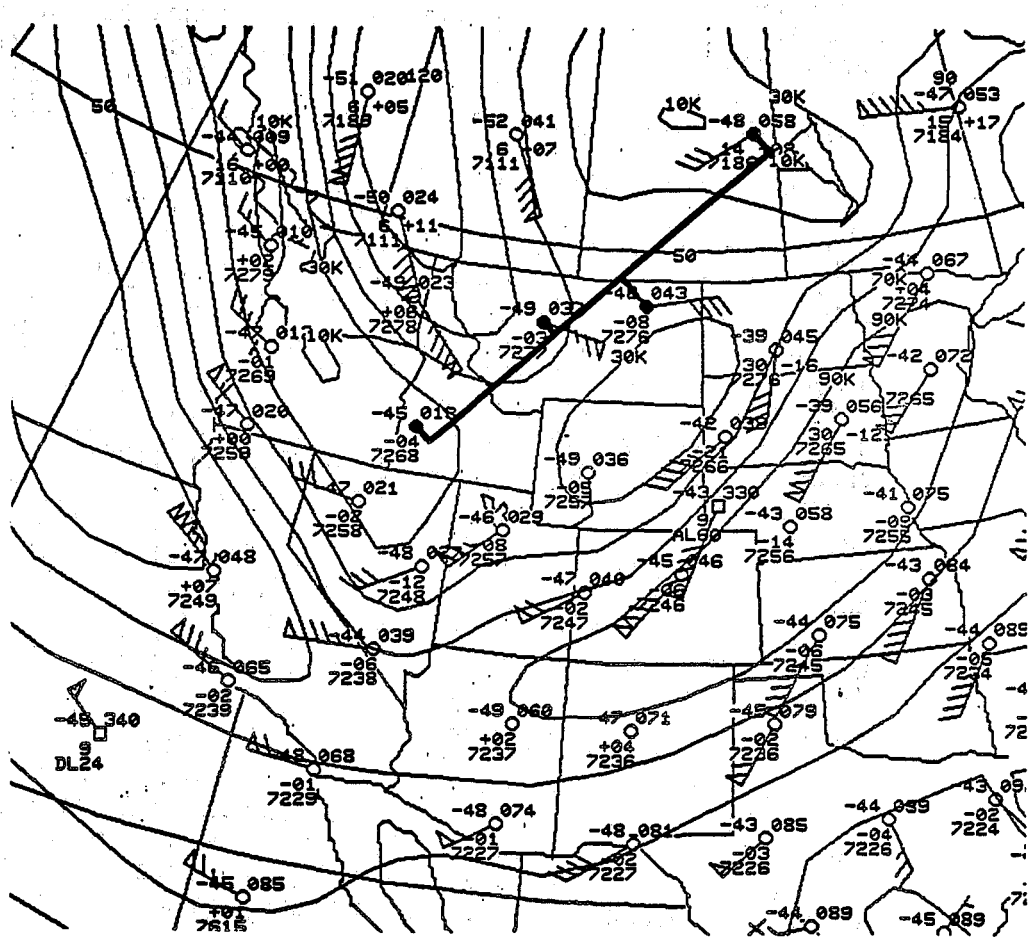

Fig. 23. 250 mb plot and isotach analysis for 1200 UTC September 25. Line AB indicates the extent of the cross section in Figure 24, with stations used indicated by the blackened centers.

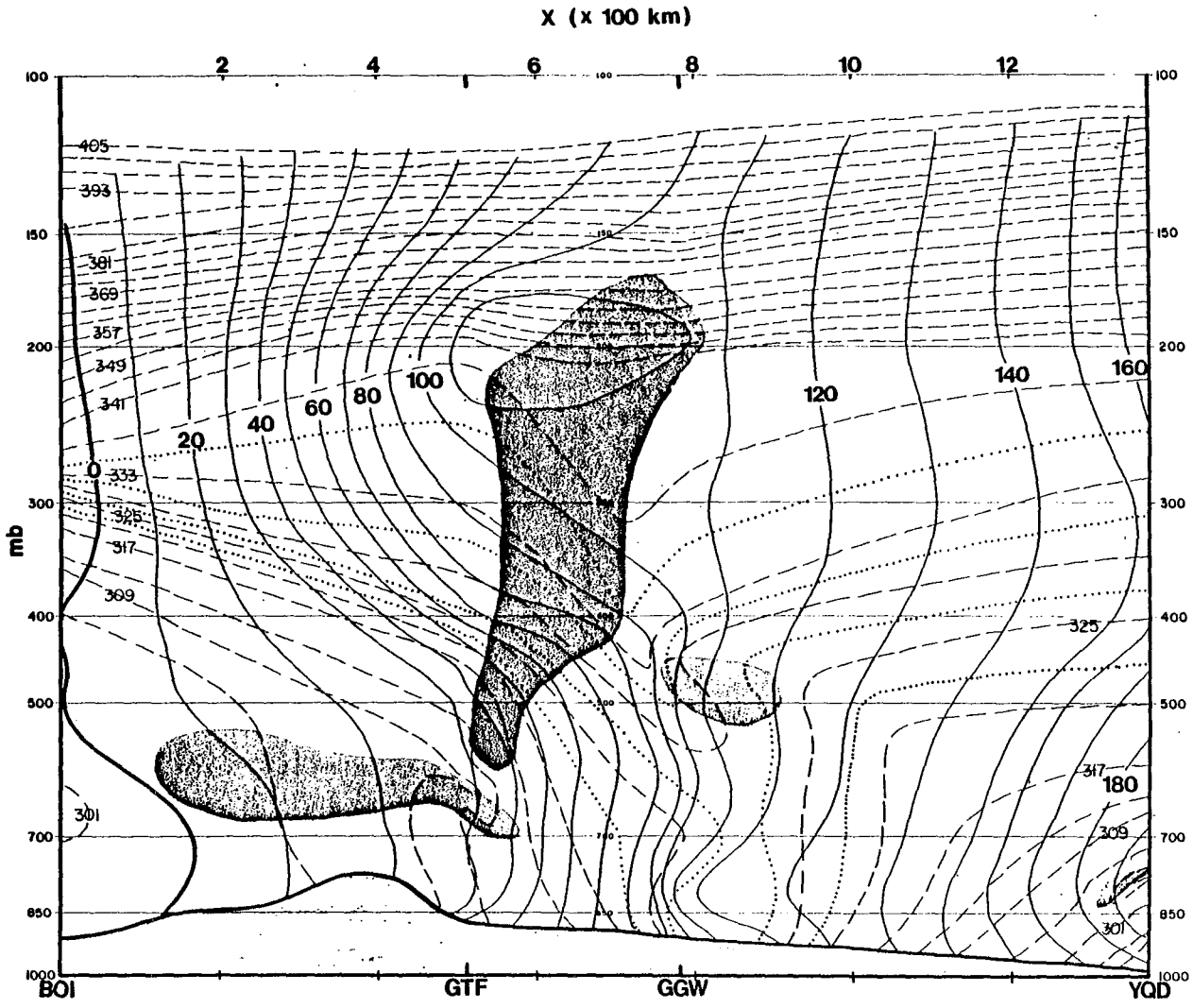

Fig. 24. Vertical cross section BOI-GTF-GGW-YQD, 1200 UTC September 25. Absolute momentum M is solid (contour interval 10 m/s), equivalent potential temperature is dashed (contour interval 4K; intermediate dotted lines yield interval of 2K across portion of cross section), and stippling indicates ares of symmetric instability.

through the Boise (BOI), Great Falls (GTF), Glasgow (GGW) and The Pas (YQD, Manitoba, Canada) cross section (as shown on Figure 23) at 1200 UTC September 25. The quantity M (= v + fx) was derived whereby v is the component of flow oriented perpendicular to the cross section, f varies with latitude and x is the distance along the cross section beginning at Boise. Those areas which are potentially unstable to slantwise motions, as described above, are stippled. It is clear that the main area susceptible to slantwise instability is between Great Falls and Glasgow - and exists throughout a significant depth of the atmosphere. This area of potential slantwise instability coincides well with the band of extreme precipitation that fell across north-central Montana at that time.

It is entirely possible, and indeed, seems likely, that such a process took place in this case to help produce the line of heavy precipitation along the baroclinic boundary, just based on the existence of the symmetric instability. It seems even more probable considering the magnitude of the localized heavy precipitation compared to the more general precipitation area, and the slightly stable nature of the available soundings adjacent to the precipitation observations. Slantwise motions probably existed across this area due to the frontogenetical forcings discussed earlier. These may have been oriented such that the symmetric instability was tapped and slantwise convection occurred.

The operational numerical models should be able to capture details such as symmetric instability and slantwise convection given that they run off the primitive equations of motion and are not limited by quasi-geostrophic restraints (such as considering relative vorticity negligible). The NGM may have precisely captured the flow field around this baroclinic zone; however, coarseness of the grid and field smoothing may have limited its intensity - thus, the precipitation amounts were too weak. Because of the grid spacing and smoothing, the minimum scale of circulation dynamics which the NGM is able to capture and represent may be near 200 km. This was approximately the scale of the ageostrophic circulation in this case as determined by the axes of maximum convergence and divergence at 1200 UTC September 25.

IV. OPERATIONAL APPLICATION OF SYMMETRIC INSTABILITY

A. Today's National Weather Service (NWS)

1. Finding Symmetric Instability

As of this writing, assessing the existence of symmetric instability is no small chore in the operational NWS environment. The tools are there to calculate the equivalent potential temperature, θ_e, and momentum, M, through a

given cross section, which appears to be the simplest method of identifying symmetric instability. No cross-sectional software has thus far been developed on the NWS AFOS system that has shown the ability to analyze enough detail through a cross section to aid the forecaster. Therefore, the ability of similar software to analyze the even greater detail sometimes present in the θ_e and momentum cross sections with enough accuracy is also suspect. It appears that the best today's operational meteorologist can do to assess the existence of symmetric instability is to plot the θ_e and momentum values through a cross section, and draw in the lines by hand. Calculating the values can be done easily on the computer.

It is also important to re-emphasize that even though symmetric instability exists, unstable motions will not occur unless slantwise motions exist such that θ_e does not increase and M does not decrease along the parcel path. Only under such conditions will slantwise convection materialize due to symmetric instability. Typically, frontogenetical forcings are important contributors in the development of these slantwise motions and therefore, observations of mesoscale or synoptic scale frontogenesis should be keys to identifying the potential for slantwise convection.

A final problem in finding symmetric instability is the time and space scales at which upper air data are currently available. An important episode of symmetric instability may exist and yet be undetectable through the radiosonde observations due to the time or location of its occurrence. Besides inference, very little can be done in such a case, and the forecaster's point of view of the existence of symmetric instability becomes more diagnostic and less predictive.

2. If Symmetric Instability Exists

Assuming the forecaster knows symmetric instability exists, how will it be reflected in the quality of the forecasts that are issued? There are probably three principle ways the products issued could be improved by knowing symmetric instability exists. First, where there is symmetric instability, precipitation may be more convective, intense and unsteady than in surrounding areas. Secondly, the location of such weather can, at times, be narrowed down more closely. Finally, the forecaster, with awareness heightened, may highlight the potential for more intense precipitation in special statements, will anticipate and watch for development in real-time, and will call for observations in the instability-prone areas.

B. The AWIPS-90 Era

1. Finding Symmetric Instability

Many of the changes proposed to take place in the NWS over the next 5 to 10 years should enhance the ability of the forecaster to identify mesoscale processes such as symmetric instability more easily. Profilers, where they are installed, will not only provide a greater density of upper air observations, but also more frequent observations. Initially, the NWS profilers may yield only wind observations. This, in itself, will help the forecaster assess the momentum surfaces more accurately and more frequently. The temperature and moisture fields, however, are also important. Unfortunately, the profilers are not nearly accurate enough nor provide enough detail in determining the thermal and humidity structures aloft for symmetric instability analysis.

There is one possible solution to this problem. Westwater and Grody (1980) and Hogg, et al. (1983) suggest that by combining profiler and VAS sounding data, a profile of the thermal and moisture characteristics may be obtained that is significantly more accurate than that produced by either system alone. These systems complement each other rather well, as each system's strengths tend to be the other's weaknesses.

2. Mesoscale Models

With the inclusion of profiler data and, possibly, satellite data in the weather service of the future, proposed operational scenarios include the addition of mesoscale numerical models that can be run at each site. With a grid spacing of 40 km or less, these models should capture details of symmetric instability more easily than today's regional models, and the result should be better guidance for the forecasters.

The future forecasting trend will be to provide more detailed and accurate short-term forecasts, especially with respect to significant weather episodes. The potential exists for both diagnostic and predictive use of symmetric instability concepts in the future of the NWS. Given better guidance and greater diagnostic confidence of the existence of symmetric instability, the forecaster should be able to put more accurate detail into the forecast than is possible today.

V. SUMMARY

The case of extreme amounts of rainfall and record flooding on September 24-25, 1986 was examined. It is hypothesized that moisture from Hurricane Newton helped not only develop the low level circulation center, but also provided the impetus for enhanced ageostrophic vertical motions along the inverted trough axis through northern Montana. The kinematic vertical velocity profiles supported 20 cm/sec ascent along the trough axis during the period of maximum rainfall, with this value being representative of an area of over 14,000 square km. Slantwise convection may have had a significant impact on the enhancement of the heaviest, flood-producing band of precipitation.

The numerical models performed rather poorly at 36 and 48 hours. Improvement was shown on the 24- and 12-hour runs, especially on the NGM. It is possible that the models improved in the shorter term because they then knew about the moisture advected into the Midwest the previous day by Hurricane Newton. Still, the best LFM forecast missed the central surface pressure by 10 mb - that from the 12-hour forecast. Neither model came close to generating the observed amounts of precipitation, though the potential was suggested.

This was an extreme event and was not an easy operational forecast in terms of the amount and precise location of the very heavy rain. The processes associated with embedded mesoscale secondary circulations and slantwise convection would have been difficult to diagnose numerically in the operational setting, though both could have been implied. Neither the Sanders and Bosart or the Emanuel articles mentioned earlier made any strong statements about how the operational community could use this new theoretical information on a real-time basis. However, under situations where slantwise parcel movement is suggested across a frontogenetic boundary, the potential should be considered, especially when the sounding observations indicate slightly stable lapse rates. In such cases, slantwise convection may also be a method which produces heavy precipitation, even when little is expected.

As shown in this case, mesoscale calculations of convergence fields may indicate the presence of slantwise parcel movement across the frontal boundary. Regular diagnostic use of convergence charts may have helped the forecaster's nowcasting effort, though any more than highlighting the potential for heavy rain and flooding in this case may have been beyond the practical capabilities given the information available.

The future does provide hope for the operational forecaster, as regional models with tighter grid spacing, operational mesoscale models and denser observation networks should capture more accurately the dynamical processes that occur. Likewise, precipitation forecasts may more accurately reflect the potential for these extreme events.

VI. ACKNOWLEDGMENTS

Input from Don Paterson, lead forecaster at Great Falls, Glenn Rasch, SSD Chief in the NWS Western Region and Ken Mielke, SSD Assistant Chief in the NWS Western Region, is greatly appreciated. Thanks also to Lance Bosart of SUNY-Albany, Kerry Emanuel of MIT and Jim Hoke from NMC for information they provided during the course of this study. They were all quite helpful and very much appreciated.

VII. REFERENCES

Emanuel, K. A., 1983a: On Assessing Local Conditional Symmetric Instability from Atmospheric Soundings. Mon. Wea. Rev., 111, 2016-2033.

Emanuel, K. A., 1983b: The Lagrangian Parcel Dynamics of Moist Symmetric Instability. J. Atmos. Sci., 40, 2368-2376.

Emanuel, K. A., 1985: Frontal Circulations in the Presence of Small Moist Symmetric Instability. J. Atmos. Sci., 42, 1062-1071.

Hogg, D. C., M. T. Decker, F. O. Guiraud, K. B. Earnshaw, D. A. Merritt, K. P. Moran, W. B. Sweezy, R. G. Strauch, E. R. Westwater and C. G. Little, 1983: An Automatic Profiler of the Temperature, Wind and Humidity in the Troposphere. J. Appl. Meteor., 22, 807-831.

Hoskins, B. J. and F. P. Bretherton, 1972: Atmospheric Frontogenesis Models: Mathematical Formulation and Solution. J. Atmos Sci., 29, 11-37.

NOAA, 1986: Precipitation, Frontogenesis and the Deformation Zone. Western Region Technical Attachment 86-15.

NOAA, 1986: RAFS Problems in the West. Western Region Technical Attachment 86-30.

Sanders, F. and L. F. Bosart, 1985: Mesoscale Structure in the Megalopolitan Snowstorm of 11-12 February 1983. Part I: Frontogenetical Forcing and Symmetric Instability. J. Atmos. Sci., 42, 1050-1061.

Westwater, E. R. and N. C. Grody, 1980: Combined Surface- and Satellite-Based Microwave Temperature Profile Retrieval. J. Appl. Meteor., 19, 1438-1444.

139 Aids for Forecasting Minimum Temperature in the Wenatchee Frost District. Robert S. Robinson, April 1979. (PB298339/AS)
140 Influence of Cloudiness on Summertime Temperatures in the Eastern Washington Fire Weather district. James Holcomb, April 1979. (PB298674/AS)
141 Comparison of LFM and MFM Precipitation Guidance for Nevada During Doreen. Christopher Hill, April 1979. (PB298613/AS)
142 The Usefulness of Data from Mountaintop Fire Lookout Stations in Determining Atmospheric Stability. Jonathan W. Corey, April 1979. (PB298899/AS)
143 The Depth of the Marine Layer at San Diego as Related to Subsequent Cool Season Precipitation Episodes in Arizona. Ira S. Brenner, May 1979. (PB298817/AS)
144 Arizona Cool Season Climatological Surface Wind and Pressure Gradient Study. Ira S. Brenner, May 1979. (PB298900/AS)
146 The BART Experiment. Morris S. Webb, October 1979. (PB80 155112)
147 Occurrence and Distribution of Flash Floods in the Western Region. Thomas L. Dietrich, December 1979. (PB80 160344)
149 Misinterpretations of Precipitation Probability Forecasts. Allan H. Murphy, Sarah Lichtenstein, Baruch Fischhoff, and Robert L. Winkler, February 1980. (PB80 174576)
150 Annual Data and Verification Tabulation - Eastern and Central North Pacific Tropical Storms and Hurricanes 1979. Emil B. Gunther and Staff, EPHC, April 1980. (PB80 220486)
151 NMC Model Performance in the Northeast Pacific. James E. Overland, PMEL-ERL, April 1980. (PB80 196033)
152 Climate of Salt Lake City, Utah. Wilbur E. Figgins, Third Revision January 1987. (PB87 157194/AS)
153 An Automatic Lightning Detection System in Northern California. James E. Rea and Chris E. Fontana, June 1980. (PB80 225592)
154 Regression Equation for the Peak Wind Gust 6 to 12 Hours in Advance at Great Falls During Strong Downslope Wind Storms. Michael J. Oard, July 1980. (PB91 108367)
155 A Raininess Index for the Arizona Monsoon. John H. Ten Harkel, July 1980. (PB81 106494)
156 The Effects of Terrain Distribution on Summer Thunderstorm Activity at Reno, Nevada. Christopher Dean Hill, July 1980. (PB81 102501)
157 An Operational Evaluation of the Scofield/Oliver Technique for Estimating Precipitation Rates from Satellite Imagery. Richard Ochoa, August 1980. (PB81 108227)
158 Hydrology Practicum. Thomas Dietrich, September 1980. (PB81 134033)
159 Tropical Cyclone Effects on California. Arnold Court, October 1980. (PB81 133779)
160 Eastern North Pacific Tropical Cyclone Occurrences During Intraseasonal Periods. Preston W. Leftwich and Gail M. Brown, February 1981. (PB81 205494)
161 Solar Radiation as a Sole Source of Energy for Photovoltaics in Las Vegas, Nevada, for July and December. Darryl Randerson, April 1981. (PB81 224503)
162 A Systems Approach to Real-Time Runoff Analysis with a Deterministic Rainfall-Runoff Model. Robert J.C. Burnash and R. Larry Ferral, April 1981. (PB81 224495)
163 A Comparison of Two Methods for Forecasting Thunderstorms at Luke Air Force Base, Arizona. LTC Keith R. Cooley, April 1981. (PB81 225393)
164 An Objective Aid for Forecasting Afternoon Relative Humidity Along the Washington Cascade East Slopes. Robert S. Robinson, April 1981. (PB81 23078)
165 Annual Data and Verification Tabulation, Eastern North Pacific Tropical Storms and Hurricanes 1980. Emil B. Gunther and Staff, May 1981. (PB82 230336)
166 Preliminary Estimates of Wind Power Potential at the nevada Test Site. Howard G. Booth, June 1981. (PB82 127036)
167 ARAP User's Guide. Mark Mathewson, July 1981, revised September 1981. (PB82 196783)
168 Forecasting the Onset of Coastal Gales Off Washington-Oregon. John R. Zimmerman and William D. Burton, August 1981. (PB82 127051)
169 A Statistical-Dynamical Model for Prediction of Tropical Cyclone Motion in the Eastern North Pacific Ocean. Preston W. Leftwich, Jr., October 1981. (PB82195298)
170 An Enhanced Plotter for Surface Airways Observations. Andrew J. Spry and Jeffrey L. Anderson, October 1981. (PB82 153883)
171 Verification of 72-Hour 500-MB Map-Type Predictions. R.F. Quiring, November 1981. (PB82 158098)
172 Forecasting Heavy Snow at Wenatchee, Washington. James W. Holcomb, December 1981. (PB82 177783)
173 Central San Joaquin Valley Type Maps. Thomas R. Crossan, December 1981. (PB82 196064)
174 ARAP Test Results. Mark A. Mathewson, December 1981. (PB82 198103)
176 Approximations to the Peak Surface Wind Gusts from Desert Thunderstorms. Darryl Randerson, June 1982. (PB82 253089)
177 Climate of Phoenix, Arizona. Robert J. Schmidli, April 1969 (revised December 1986). (PB87 142063/AS)
178 Annual Data and Verification Tabulation, Eastern North Pacific Tropical Storms and Hurricanes 1982. E.B. Gunther, June 1983. (PB85 106078)
179 Stratified Maximum Temperature Relationships Between Sixteen Zone Stations in Arizona and Respective Key Stations. Ira S. Brenner, June 1983. (PB83 249904)
180 Standard Hydrologic Exchange Format (SHEF) Version I. Phillip A. Pasteries, Vernon C. Bissel, David G. Bennett, August 1983. (PB85 106052)
181 Quantitative and Spacial Distribution of Winter Precipitation along Utah's Wasatch Front. Lawrence B. Dunn, August 1983. (PB85 106912)
182 500 Millibar Sign Frequency Teleconnection Charts - Winter. Lawrence B. Dunn, December 1983. (PB85 106276)
183 500 Millibar Sign Frequency Teleconnection Charts - Spring. Lawrence B. Dunn, January 1984. (PB85 111367)
184 Collection and Use of Lightning Strike Data in the Western U.S. During Summer 1983. Glenn Rasch and Mark Mathewson, February 1984. (PB85 110534)
185 500 Millibar Sign Frequency Teleconnection Charts - Summer. Lawrence B. Dunn, March 1984. (PB85 111359)
186 Annual Data and Verification Tabulation eastern North Pacific Tropical Storms and Hurricanes 1983. E.B. Gunther, March 1984. (PB85 109635)
187 500 Millibar Sign Frequency Teleconnection Charts - Fall. Lawrence B. Dunn, May 1984. (PB85 110930)
188 The Use and Interpretation of Isentropic Analyses. Jeffrey L. Anderson, October 1984. (PB85 132694)
189 Annual Data & Verification Tabulation Eastern North Pacific Tropical Storms and Hurricanes 1984. E.B. Gunther and R.L. Cross, April 1985. (PB85 1878887AS)
190 Great Salt Lake Effect Snowfall: Some Notes and An Example. David M. Carpenter, October 1985. (PB86 119153/AS)
191 Large Scale Patterns Associated with Major Freeze Episodes in the Agricultural Southwest. Ronald S. Hamilton and Glenn R. Lussky, December 1985. (PB86 144474AS)
192 NWR Voice Synthesis Project: Phase I. Glen W. Sampson, January 1986. (PB86 145604/AS)
193 The MCC - An Overview and Case Study on Its Impact in the Western United States. Glenn R. Lussky, March 1986. (PB86 170651/AS)
194 Annual Data and Verification Tabulation Eastern North Pacific Tropical Storms and Hurricanes 1985. E.B. Gunther and R.L. Cross, March 1986. (PB86 170941/AS)
195 Radid Interpretation Guidelines. Roger G. Pappas, March 1986. (PB86 177080/AS)
196 A Mesoscale Convective Complex Type Storm over the Desert Southwest. Darryl Randerson, April 1986. (PB86 190998/AS)
197 The Effects of Eastern North Pacific Tropical Cyclones on the Southwestern United States. Walter Smith, August 1986. (PB87 106258AS)
198 Preliminary Lightning Climatology Studies for Idaho. Christopher D. Hill, Carl J. Gorski, and Michael C. Conger, April 1987.

NOAA SCIENTIFIC AND TECHNICAL PUBLICATIONS

The National Oceanic and Atmospheric Administration was established as part of the Department of Commerce on October 3, 1970. The mission responsibilities of NOAA are to assess the socioeconomic impact of natural and technological changes in the environment and to monitor and predict the state of the solid Earth, the oceans and their living resources, the atmosphere, and the space environment of the Earth.

The major components of NOAA regularly produce various types of scientific and technical information in the following kinds of publications:

PROFESSIONAL PAPERS — Important definitive research results, major techniques, and special investigations.

CONTRACT AND GRANT REPORTS — Reports prepared by contractors or grantees under NOAA sponsorship.

ATLAS — Presentation of analyzed data generally in the form of maps showing distribution of rainfall, chemical and physical conditions of oceans and atmosphere, distribution of fishes and marine mammals, ionospheric conditions, etc.

TECHNICAL SERVICE PUBLICATIONS — Reports containing data, observations, instructions, etc. A partial listing includes data serials; prediction and outlook periodicals; technical manuals, training papers, planning reports, and information serials; and miscellaneous technical publications.

TECHNICAL REPORTS — Journal quality with extensive details, mathematical developments, or data listings.

TECHNICAL MEMORANDUMS — Reports of preliminary, partial, or negative research or technology results, interim instructions, and the like.

Information on availability of NOAA publications can be obtained from:

ENVIRONMENTAL SCIENCE INFORMATION CENTER (D822)
ENVIRONMENTAL DATA AND INFORMATION SERVICE
NATIONAL OCEANIC AND ATMOSPHERIC ADMINISTRATION
U.S. DEPARTMENT OF COMMERCE

6009 Executive Boulevard
Rockville, MD 20852